Air Force Institute of Technology
AFIT Scholar

Theses and Dissertations

3-23-2017

# Optimal Configurations for Aerosol Monitoring with Multi-Rotor Small Unmanned Aerial Systems

Inna D. Chavez

Follow this and additional works at: https://scholar.afit.edu/etd

Part of the Industrial Technology Commons

Recommended Citation
Chavez, Inna D., "Optimal Configurations for Aerosol Monitoring with Multi-Rotor Small Unmanned Aerial Systems" (2017). *Theses and Dissertations*. 809.
https://scholar.afit.edu/etd/809

This Thesis is brought to you for free and open access by AFIT Scholar. It has been accepted for inclusion in Theses and Dissertations by an authorized administrator of AFIT Scholar. For more information, please contact richard.mansfield@afit.edu.

# OPTIMAL CONFIGURATIONS FOR AEROSOL MONITORING WITH MULTI-ROTOR SMALL UNMANNED AERIAL SYSTEMS

THESIS

Inna D. Chavez, Capt., USAF

AFIT-ENV-MS-17-M-179

**DEPARTMENT OF THE AIR FORCE**
**AIR UNIVERSITY**

**AIR FORCE INSTITUTE OF TECHNOLOGY**

**Wright-Patterson Air Force Base, Ohio**

**DISTRIBUTION STATEMENT A.**
APPROVED FOR PUBLIC RELEASE; DISTRIBUTION UNLIMITED.

The views expressed in this thesis are those of the author and do not reflect the official policy or position of the United States Air Force, Department of Defense, or the United States Government. This material is declared a work of the U.S. Government and is not subject to copyright protection in the United States

AFIT-ENV-MS-17-M-179

# OPTIMAL CONFIGURATIONS FOR AEROSOL MONITORING WITH MULTI-ROTOR SMALL UNMANNED AERIAL SYSTEMS

THESIS

Presented to the Faculty

Department of Systems Engineering and Management

Graduate School of Engineering and Management

Air Force Institute of Technology

Air University

Air Education and Training Command

In Partial Fulfillment of the Requirements for the

Degree of Master of Science in Industrial Hygiene

Inna D. Chavez, BS

Captain, USAF

March 2017

**DISTRIBUTION STATEMENT A.**
APPROVED FOR PUBLIC RELEASE; DISTRIBUTION UNLIMITED.

AFIT-ENV-MS-17-M-179

OPTIMAL CONFIGURATIONS FOR AEROSOL MONITORING
WITH MULTI-ROTOR SMALL UNMANNED AERIAL SYSTEMS

Inna D. Chavez, BS

Captain, USAF

Committee Membership:

Lt Col R. M. Eninger, PhD
Chair

Dr. K. H. Dunn, ScD
Member

Dr. J. M. Slagley, PhD
Member

AFIT-ENV-MS-17-M-179


## Abstract

Applicability of aerosol sampling on multi-rotor unmanned aerial systems (UAS) platform was investigated. Multi-rotor UAS have impacts of wind speed, turbulence, and orientation possibly contributing to sampling bias. The SKC IMPACT sampler, Tecora C.A.Th.I.A., and modified three-dimensionally printed *Universal Inlet for Airborne-Particle Size-Selective Sampling* were selected based on particle size-selectivity and operational independence to wind. Airflow visualizations concluded that below UAS fuselage was optimal sampler placement.

Tests were conducted with Arizona Road Dust in a still-air chamber, and aerosolized sugar in a wind tunnel. Inlet mounting was evaluated in, upright, upside-down, and horizontal orientations. Horizontal orientations of all inlets resulted in negative sampling bias compared to upright/upside-down positions. Sampling bias of inlets mounted on the UAS were compared with and without motor employment. In wind tunnel tests, the IMPACT sampler averaged lowest count concentration bias while the 3D printed inlet resulted in the largest percent difference. Results suggests, UAS turbulence and low wind speed produced negative sampling bias.

The 3D printed inlet was designed with Stokes' scaling factor, and compared with the well-characterized IMPACT sampler. Three-dimensional printing bolstered a cost-effective and fast method of inlet design and construction. Iterative designs can optimize aerosol inlets suitable for mounting on multi-rotor UAS.

**Acknowledgements**

I would like to express my sincere appreciation to those who contributed to the completion of this thesis.

To my academic and research advisor, Lt Col Robert Eninger, for his guidance and supportive patience throughout the course of my research and graduate program. His insight and experience has certainly encouraged me to continue growing academically and professionally.

I also extend my gratitude to Dr. Kevin Dunn, whose investment of time and effort supported my research from the very beginning. Dr. Jeremy Slagley who embraced my research efforts with enthusiasm and great insight as soon as he arrived at AFIT. Special thanks to Dr. Justin Clinton and Mr. Jeremy Gray for their support and subject matter expertise on the UAS. Dr. Christin Grabinski and Ms. Megan Steele, for allowing me to utilize their resources and equipment which helped me move forward in experimental method development. Captain William Page, for his assistance and knowledge with 3D printing. Dr. Sergey Grinshpun and Dr. Michael Yermakov, for their diligence and assistance in data collection. Dr. Steven Guffey and Dr. Kevin He for allowing me to use their wind tunnel.

To Hervey, for his endless encouragement and unyielding patience. I could not have asked for a more inspiring support system as we move towards the next chapter in our lives. Most importantly, to my parents, for the steadfast love and support in everything I've aimed to endeavor.

Inna D. Chavez

## Table of Contents

Page

Abstract ..... v
Acknowledgements ..... vi
Table of Contents ..... vii
List of Figures ..... ix
List of Tables ..... xiii
List of Equations ..... xiii
I. Introduction ..... 1
Background ..... 1
Problem Statement ..... 2
Justification ..... 3
Assumption/Scope ..... 4
Standards ..... 4
Approach/Methodology ..... 5
Research Question ..... 6
Materials/Equipment ..... 6
Chapter Preview ..... 7
II. Literature Review ..... 8
Chapter Overview ..... 8
UAS Background ..... 8
Subcomponent Aerosol Sampling Attributes ..... 11
III. Methodology ..... 23
Chapter Overview/Introduction: ..... 23

Applicability of UAS as a Sampling Platform .....23

Small Unmanned Aerial System .....24

Procedures and Processes .....26

IV. Results.....41

Airflow Visualization .....41

Aerosol Chamber Concentration Distribution.....45

Aerosol Inlet Orientations .....48

Aerosol Inlet Mounted on UAS (On vs. Off) .....55

V. Discussion .....69

Specific Aim 1 Revisited.....69

Specific Aim 2 Revisited.....70

Specific Aim 3 Revisited.....70

Summary.....72

VI. 3D Printed Universal Inlet .....74

Introduction .....74

Design Process.....74

Design Modifications .....75

Inlet Characterization .....77

Results .....81

Summary.....82

VII. Conclusion.....83

Bibliography .....84

## List of Figures

Page

Figure 1. IMPACT Sampler from SKC Inc. (SKC IMPACT sampler, 2016)..... 15

Figure 2. Airstream Lines of IMPACT Sampler (Diagram courtesy of SKC, Inc.)..... 15

Figure 3. Sampling Efficiency Curve for IMPACT sampler (Diagram courtesy of SKC, Inc.) ..... 16

Figure 4. C.A.Th.I.A Sampler from Tecora (Tecora C.A.Th.I.A, 2016)..... 17

Figure 5. CATHIA Airstream Flow (Diagram courtesy of Tecora, SLR)..... 18

Figure 6. CATHIA Efficiency Curve (Diagram courtesy of Tecora, SLR)..... 18

Figure 7. Universal Inlet For Airborne-Particle Size-Selective Sampling by Raabe et al. (Raabe & Teague, 1995) ..... 19

Figure 8. Photograph of Multi-rotor UAS with CATHIA Mounted..... 26

Figure 9. NIOSH Tracer Gas Room Diagram of UAS Airflow Visualization Setup – Planar View (Modified diagram courtesy of NIOSH Division of Applied Research and Technology)..... 29

Figure 10. Airflow Visualization Setup ..... 30

Figure 11. Aerosol Generator with Three Nebulizers..... 31

Figure 12. Test Setup of UAS On vs. Off Comparisons – Planar View..... 32

Figure 13. Planar View of Aerosol Inlet Mounting Location on UAS, A. SKC PM10 IMPACT Location, B. 3D Printed Inlet and CATHIA Location (Not to scale) ..... 33

Figure 14. Elevated View of Aerosol Inlet Mounting Location on UAS, A. SKC PM10 IMPACT Location, B. 3D Printed Inlet and CATHIA Location (Not to scale) ..... 33

Figure 15. West Virginia University Wind Tunnel (Diagram courtesy of Industrial & Management Systems Engineering West Virginia University) ..... 36

Figure 16. Test Setup of UAS On vs. Off Comparisons in WVU Wind Tunnel – Planar View (Not to scale) ..... 37

Figure 17. Beginning of Fog Generation with Propellers Off ..... 42

Figure 18. Initial Airflow Movement with Propellers On ..... 42

Figure 19. Airflow Movement after 1.02 seconds with Propellers On ..... 43

Figure 20. Airflow Movement after 2.02 seconds with Propellers On ..... 43

Figure 21. Airflow Movement after 2.02 seconds with Overlay of Instantaneous Vertical Downward Velocity Contours (Overlay image modified from Hwang et al., 2015). 44

Figure 22. Complete Mixing after 6.06 seconds with Propellers On ..... 45

Figure 23. Overlay Plot of Aerosol Concentration in UC Chamber with GRIMM..... 46

Figure 24. Histogram Plot of Aerosol Concentration in UC Chamber with GRIMM..... 46

Figure 25. Particle Count Concentration from CPC Taken Over Time in WVU Wind Tunnel ..... 47

Figure 26. Histogram Plot of Aerosol Concentration in WVU Chamber with CPC ..... 48

Figure 27. SKC IMPACT Sampler Orientation Comparisons with ARD ..... 49

Figure 28. CATHIA Orientation Comparisons with ARD ..... 50

Figure 29. 3D Printed Inlet Orientation Comparisons with ARD ..... 50

Figure 30. Orientation Comparisons of SKC IMPACT SAMPLER, CATHIA, and 3D Printed Inlet with ARD ..... 51

Figure 31. Comparison of 3D Printed Inlet vs. SKC IMPACT SAMPLER in 0.254 m/s Wind Speed and Sugar Test Aerosol ..... 52

Figure 32. One-way Analysis of 2.458 µm by CATHIA Inlet Orientations with ARD... 54

Figure 33. One-way Analysis of 3.051 µm by CATHIA Inlet Orientations with ARD... 54

Figure 34. One-way Analysis of 9.647 µm by 3D Printed Inlet Orientations with ARD. 55

Figure 35. UAS On vs Off Comparison for SKC IMPACT Sampler with ARD..... 57

Figure 36. UAS On vs Off Comparison for 3D Printed Inlet with ARD..... 58

Figure 37. UAS On vs Off Comparison for CATHIA with ARD ..... 59

Figure 38. UAS On vs Off Comparison for SKC IMPACT Sampler, 3D Printed Inlet, and CATHIA with ARD ..... 60

Figure 39. Particle Count Percent Difference UAS On vs Off Comparison for Inlets with ARD in UC Aerosol Chamber with 95% Confidence Interval (combined size bins) 61

Figure 40. Measure of Central Tendency of Particle Count Percent Difference UAS On vs Off Comparison for Inlets with ARD in UC Aerosol Chamber (smooth lines).... 62

Figure 41. UAS On vs Off Comparison for SKC IMPACT Sampler with Sugar and 0.254 m/s Wind Tunnel Speed ..... 63

Figure 42. UAS On vs Off Comparison for 3D Printed Inlet with Sugar and 0.254 m/s Wind Tunnel Speed..... 64

Figure 43. UAS On vs Off Comparison for CATHIA with Sugar and 0.254 m/s Wind Tunnel Speed..... 65

Figure 44. Particle Count Concentration UAS On vs Off Comparison for SKC IMPACT Sampler, 3D Printed Inlet, and CATHIA with Sugar and 0.254 m/s Wind Tunnel Speed ..... 66

Figure 45. Percent Difference UAS On vs Off Comparison for SKC IMPACT SAMPLER, 3D Printed Inlet, CATHIA with Sugar and 50 FPM Wind Tunnel Speed with 95% Confidence Interval (combined bins) ..... 67

Figure 46. Measure of Central Tendency of Percent Difference UAS On vs Off Comparison for SKC IMPACT SAMPLER, 3D Printed Inlet, CATHIA with Sugar and 0.254 m/s Wind Tunnel Speed (smooth lines) ..... 68

Figure 47. Exploded View of Six Component 3D Printed Inlet ..... 76

Figure 48. Assembled 3D Printed Inlet ..... 77

Figure 49. Top View of Calibration Jar ..... 78

Figure 50. 3D Printed Inlet Calibration Jar ..... 79

Figure 51. Side-by-side comparison of initial design (left) and revised design (right) of Base Plate ..... 79

Figure 52. Side-by-side comparison of initial design (left) and revised design (right) of Fan Plate ..... 80

Figure 53. Side-by-side comparison of initial design (left) and revised design (right) of Bell Cap ..... 80

Figure 54. One-way Analysis of 2.129 µm by 3D Printed Inlet and SKC IMPACT SAMPLER with ARD ..... 81

Figure 55. 3D Printed Inlet and SKC IMPACT SAMPLER Comparison with ARD ..... 82

## List of Tables

Table 1. Test Condition Summary for Experiment 2 and 3 ..... 40

Table 2. Combined P-Values of Aerosol Inlet Orientation Comparisons ..... 52

Table 3. Combined P-Values of UAS "On" vs. "Off" Comparisons ..... 68

## List of Equations

Equation 1. Stokes' Number ..... 13

Equation 2. Stokes' Number as Ratio of Particle Stop Distance to Dimensional Scale of Flow Distortion ..... 13

Equation 3. Fisher's Method For Combining P-Values…….....39

Equation 4. Percent Difference ..... 39

Equation 5. Effective Cutoff Aerodynamic Diameter For Stokes Inlet Scaling……75

# OPTIMAL CONFIGURATIONS FOR AEROSOL MONITORING WITH MULTI-ROTOR SMALL UNMANNED AERIAL SYSTEMS

## I. Introduction

### Background

Unmanned aircraft systems (UAS), unmanned aerial vehicles (UAVs), and remotely piloted aircraft (RPA) have a contributing history in their support of military warfare efforts. As the technology evolves, the widespread application of UAS covers a large array of applications in commercial use to environmental monitoring. Although the evolution of UAS technology was spearheaded primarily for the purposes of military operations, the applicability among civilian users for the purposes of earth sensing reconnaissance and scientific data collection is becoming more widespread (Watts et al., 2012). Particularly for contaminant sampling, detection, characterization, and remote sensing, UAS is a promising, flexible and mobile platform (Eninger and Johnson, 2015). With respect to the application of scientific investigation, different models of UAS are advantageous for diverse applications and have been utilized in environmental monitoring across a wide variety of applications.

A fixed-wing, unmanned aircraft is suitable for extended flight time over a long distance, while multi-rotor systems are practical for smaller mapping areas or for stationary monitoring (Harriman and Muhlhausen, 2013). To obtain a sampling of the aerosol concentration and composition over a specific location, a monitor is required to dwell over the area for a longer period of time, making the use of a rotor-based UAS a

practical choice. Using UAS in the collection of atmospheric aerosol sampling continues to gain in popularity (Craft et al., 2014). Demonstrations on unmanned aircraft of varying size and capability have proven to be successful to support measurements of trace gases, aerosols, and dynamics of the upper troposphere and lower stratosphere. The potential for revolutionizing scientific observations is promising, and the continued utility of UAS technology in the realm of occupational hygiene and aerosol monitoring should be further explored (Eninger and Johnson, 2015).

Although aerosol collection utilizing fixed-wing UAS air frames has been well characterized, the use of small, multi-rotor UAS airframes as platforms for aerosol sampling and monitoring requires more in-depth investigation. An advantage that multi-rotor UAS have is the ability to run on electric power, thus eliminating the effects on the aerosol sampling from the aircraft emissions. However, critical design considerations must be addressed to determine optimal configurations for UAS airframes and aerosol sampling instruments.

## Problem Statement

Though multi-rotor UAS have the advantage of running on electric power to eliminate the effects on aerosol sampling from the aircraft emissions, impacts of wind speed, turbulence, and orientation may bias aerosol sampling results. Complex proximate air flow from multi-rotor propulsion and dynamic flight profile may bias particle samplers employed on small UAS. Valid air sampling requires accurate, precise, and well-characterized particle size fractioning or isokinetic aerosol collection. The

placement of the airborne aerosol inlets is important to minimize the influence of the aircraft on the sample aerosol (Hermann et al., 2001). Critical design considerations must be addressed to determine optimal configurations for UAS airframes and aerosol sampling instruments. Although aerosol collection on fixed-wing aircraft in forward flight is fairly well-characterized, a gap in the literature exists in the area of aerosol collection and sampling bias using multi-rotor UAS as a sampling platform. The particle inertial effects and environmental influences of UAS as an air sampling platform are understood to possibly bias aerosol sampling. What is lacking is an orientation-averaged particle size sampling bias characterization covering a hypothesized complex flight profile of a UAS.

**Justification**

This research has direct impact to environmental, health and safety industries. The US Environmental Protection Agency, National Institution for Occupational Safety and Health (NIOSH), fire and rescue teams, and DoD operations will benefit from this research. Particularly in US Air Force operations, Emergency Management, Bioenvironmental Engineers, and industrial hygienists have the tasks characterizing and performing health risk evaluations. These personnel utilize aerosol monitoring to complete their respective tasks. However, they are often subjected to hazardous exposures in the collection of aerosol samples. Using UAS as a sampling platform may eliminate or minimize the need for personnel to enter into the hazardous environments for aerosol sampling. The environmental, health and safety agencies would materially

benefit from a UAS-borne aerosol sampling capability. Once optimal configurations for aerosol particle collection on a multi-rotor small UAS are determined, an understanding of the sampling bias limitations will be gained. This research will contribute to the understanding of aerosol sampling and collection using contemporary multi-rotor UAS as a sampling platform.

**Assumption/Scope**

The objectives in the sampling of this work are not to determine health hazard exposures or compliance, but to investigate the applicability of aerosol sampling on a multi-rotor unmanned aerial systems (UAS) platform. The UAS platform will create a turbulent sampling environment and likely have influence on these sampling parameters. Utilizing the UAS platform will also limit sampling time due to the power and flight time of the UAS. This study will be limited to three candidate omnidirectional aerosol sampling inlets and the small multi-rotor UAS produced by the Air Force Institute of Technology Autonomy and Navigation Technology (ANT) Center. A detailed description of the UAS used in this research is further explained in Chapter 3. The design and production parameters, along with any navigation, sensoring, or electrical power determination of a small multi-rotor UAS are beyond the scope of this study.

**Standards**

Particle size-selective sampling is the collection of different sized particles that may penetrate and adversely affect regions of the respiratory tract. The thoracic fraction is the mass fraction particles with the potential to penetrate beyond the larynx. The

American Conference of Governmental Industrial Hygienists (ACGIH) recommends particle size-selective sampling in setting threshold limit values for occupational exposures and established criteria for Inhalable, Thoracic, and Respirable Particulate Mass fractions. Stokesian properties (the hydrodynamic and nonhydrodynamic behavior of particles when they are suspended in a fluid medium) of a particle are a key measurement in an airborne particle's ability to move through air (Brady, 1988). Both the Stokesian properties and current industrial hygiene industry standards for aerosol monitoring for particle size selective inlets of thoracic cut points were considered in the application of this research.

**Approach/Methodology**

Sampling bias of inlets when mounted on the UAS sampling platform were compared with and without the employment of the UAS rotors. Existing research and commercial aerosol samplers were identified for their possible efficacy on small UAS airframes. Inlets were selected based on particle size selectivity and operational independence to wind speed and direction. Selected inlets were first characterized in an aerosol chamber to compare their limitations and capabilities at varying orientations. High-flow rate air sampling pumps were selected with special consideration for UAS payload limitations. A critical assessment of existing aerosol collection instruments with a focus on employability for use on a small UAS airframe was conducted. The results of the inlet characterization while mounted on the UAS platform with motors off served as the expected reference sampling efficiency and was compared to the observed sampler collected value with the motors turned on.

## Research Question

The objective of this research was to contribute to the understanding of aerosol sampling and collection bias using a contemporary multi-rotor UAS as a sampling platform. Optimal configurations for aerosol particle collection on a multi-rotor, small UAS were determined. These objectives were accomplished by completing the following three specific aims:

Specific Aim 1: *Small multi-rotor UAS airframe airflow characterization.* Critically evaluate ideal placement and orientation of aerosol particle collection devices.

Specific Aim 2: *Assess existing and modified aerosol collections designs to minimize aspiration bias*. Key considerations included the effects of wind speed, turbulence, orientation, and sampler flow rate on particle aspiration. Sampling pump, sampler inlet, and potential modifications were reviewed to improve sampling performance.

Specific Aim 3: *Sampling bias determination for UAS airframe and aerosol sampler in hovering and forward flight.* Particle size sampling bias characterization was produced for UAS forward and hovering flight in calm air environment.

## Materials/Equipment

The materials and equipment used in this study were conducted in an aerosol test chamber and large wind tunnel and include experimental setup supplies (sampler filters,

tubing, connectors, and air flow splitters), aerosol samplers, air sampling pump, and aerodynamic particle sizer (APS). A detailed description of the materials used is further expanded in Chapter 3.

**Chapter Preview**

Chapter 2 reviews the basic principles covering aerosol sampling on a UAS in forward flight, an example on a multi-rotor system, the benefits of a multi-rotor system as a sampling platform, and the subcomponent attributes of aerosol sampling. Chapter 3 outlines the experimental method for determining the sampling efficiencies of selected aerosol inlets mounted on an unmanned aerial system. Chapters 4 summarizes the results and analysis of sampling efficiency data. Chapter 5 provides an in-depth analysis of the 3D printed universal air sampling inlet.

# II. Literature Review

## Chapter Overview

Although the evolution of UAS technology was spearheaded primarily for the purposes of military operations, the applicability among civilian users for the purposes of earth sensing reconnaissance and scientific data collection is becoming more widespread (Watts et al., 2012). With respect to the application of scientific investigation, different models of UAS are advantageous for different applications. Fixed wing unmanned aircraft are more suitable for extended flight time over a long distance, while multi-rotors (i.e. quad-rotors) are more practical for smaller mapping areas or the need for stationary monitoring (Harriman and Muhlhausen, 2013). Chapter 2 reviews the basic principles covering aerosol sampling on a UAS in forward flight, an example on a multi-rotor system, the benefits of a multi-rotor system as a sampling platform, and the subcomponent attributes of aerosol sampling.

## UAS Background

A number of demonstrations on unmanned aircraft of varying size and capability have proven to be successful to support measurements of trace gases, aerosols and dynamics of the upper troposphere and lower stratosphere.

In studies conducted for aerosol collection in forward flight on fixed-wing UAS airframes, the placement of sensors and inlets were investigated (Bernard and Krispin, 2010 and Hermann et al., 2001). Hermann et al.'s study utilized direct reading instruments to sample aerosol particles from aircraft with simultaneous measurement of

trace gases (e.g., carbon monoxide (CO), ozone ($O_3$), methane ($CH_4$), chlorofluorocarbons (CFCs), hydrochlorofluorocarbons (HCFCs)). It was determined that the inlet system was the most critical item because of its strong variability in modifying the number concentration, size distribution, and chemical composition of the particles. The placement of the airborne aerosol inlets and sensors was also important, so that the influence of the aircraft on the sample aerosol was minimized (Bernard and Krispin, 2010 Hermann et al., 2001).

Other investigations of trace gas and aerosol sampling on fixed-wing UAS were conducted in studies by Watts et al., Craft et al., and Corrigan et al. The Right-of Way Automated Monitoring-Greenhouse Gas Mission (RAM-GGM) pilot study focused on test bed instruments for autonomously detecting and locating methane releases from petroleum production, extraction sites, and distribution networks. A Cavity-Ring Flux Analyzer onboard the aircraft was successful in mapping methane levels in the lower atmosphere in Railroad Valley (Watts et al., 2012). Scientists from the University of Alaska Fairbanks, the University of California, Davis, and Arizona State University conducting the Prescribed Fire Combustion and Atmospheric Dynamics Research Experiment at Eglin Air Force Base, Florida validated utility of UAS in fire mapping applications to monitor the smoke plume and burning behavior of fires (Craft et al., 2014). Corrigan et al. investigated the interaction of aerosol, clouds, and radiative effects (Corrigan et al., 2008). Miniaturized instruments were used on UAS to determine routine vertical profiles of aerosol and water vapor; these instruments collected measurements of

total particle concentration, particle size distributions, aerosol absorption and black carbon concentrations (Corrigan et al., 2008).

Investigations of multi-rotor UAS utility as an aerosol sampling platform have been presented by Altstädter et al., Brady et al., and Chang et al. Altstädter et al. developed the Application of Light-weight aircraft for Detecting In-situ Aerosol equipped with direct reading instruments. Their work concluded that measured concentrations from the multi-rotor UAS were consistent with the measurements from a scanning mobility particle sizer (SMPS) and aerodynamic particle sizer (APS) located at ground level. In a study conducted by Chang et al., a multi-rotor UAS was designed with the air sampling techniques of an evacuated canister to demonstrate its field applicability. The major advantages resulting from the study demonstrated that first, the maneuverability of the multi-rotor coupled with and air sampler can be readily deployed for environmental studies. Second, the aerial sampling and preservation conditions can be performed at desired positions. And third, data for a large array of vertical profiles of gaseous species can be easily obtained (Chang et al., 2015). Brady et al characterized a commercial quadrotor UAS as a sampling platform to measure vertical and horizontal profiles of aerosol particle and $CO_2$ concentrations at a coastal site in Southern California. Using an Iris UAS, they were able to find that the mobile platform provided efficient and precise measurements in the vertical and horizontal profiles of sea spray aerosol generated within the boundary layer.

Researchers continue to characterize the utilization of UAS in engineering and environmental industries and its abilities in contamination monitoring. Current

measurement platforms include fixed tall towers, tethered balloons, and fixed winged UASs. The use of multi-rotor UASs introduces a low-cost alternative sampling platform. These multi-rotor UASs have the advantage of a capability to hold a fixed position in areas that could potential involve high risk of human life. To obtain a sampling for the aerosol concentration and composition over a specific location, a monitor is required to dwell over the area for a longer period of time, making the use of UAS a practical choice. An advantage that UAS have is its ability to run on electric power, thus eliminating the effects on the aerosol sampling from the aircraft emissions. With respect to the application of scientific investigation, different models of UAS are advantageous for different applications. A fixed wing unmanned aircraft is more suitable for extended flight time over a long distance, while multi-rotor systems are more practical for smaller mapping areas or the need for stationary monitoring (Harriman and Muhlhausen, 2013).

Although aerosol sampling on fixed-wing UAS are fairly well-characterized, a critical design considerations for small multi-rotor airframes is lacking in literature.

**Subcomponent Aerosol Sampling Attributes**

The subcomponent aerosol sampling attributes include sampling inlet selection and candidate inlet characterization. The three candidate sampling inlets are the SKC IMPACT sampler, Tecora C.A.Th.I.A., and a modified 3-D printed *Universal Inlet for Airborne-Particle Size-Selective Sampling* based on the US Patent design of Raabe et al. A detailed description of the 3-D printed inlet modification are expanded in Chapter 5. The effects of sampling efficiencies, bluff bodies, and thoracic and respirable particle penetration are also described in more detail.

## Sampling Inlets

Prior to selecting sample measurement methods and media, it is important to first define the sampling objectives. The objectives in the sampling of this work were not to determine health hazard exposures or compliance, but rather to investigate the applicability of aerosol sampling on a multi-rotor unmanned aerial systems (UAS) platform. Sampling parameters that need consideration included, flow rate, sample volume, and sampling time. The UAS platform will create a turbulent sampling environment and likely have influence on these sampling parameters. Utilizing the UAS platform will limit sampling time to less than 30 minutes; it is desirable to select high flow rate samplers, which are appropriate for both low airborne particle concentrations and short-term exposure measurements (Lee et al., 2010). The sampling efficiency of air samplers will be significantly different in moving air compared to calm air environments (Gorner et al, 2009). To account for the effects of moving air, it is important to evaluate air sampling inlets that are generally independent of wind speed and direction (Volkwein, 2011).

In studies of different aerosol samplers, it was demonstrated that the aspiration efficiency was dependent on particle aerodynamic diameter and state of electrical charge (Gorner et al, 2009). The high efficiency CIP 10-Inhalable aerosol sampler meets fairly well the conventional CEN/ISO-ACGIH criteria for sampling the inhalable health-related aerosol fraction (Gorner et al, 2009). An omni-directional sampling slot has the same efficiency when rotating or not and, in the workplace, it is expected to operate with an

efficiency similar to that measured experimentally (Gorner et al, 2009). The 50% cutpoints for the respirable and thoracic conventions are 4 and 10 µm respectively (Baron, 2016). Where high air velocities are expected, samplers with a sampling efficiency that are not as prone to wind speed should be selected. Aerosol sampling inlets expected to have the least sampling bias and closest adherence to the thoracic curve and PM10 particle size selective conventions were considered for this research.

**Candidate inlets**

The Stokesian properties of a particle are a key attribute in an airborne particle's ability to move through air (the effects of particle inertia). The effects of particle inertia demonstrate particle aerodynamic diameter and its direct relationship to particle motion.

Stokes' number is a dimensionless quantity defined as

$$St = \frac{d^2 \rho U}{18 \mu D} \tag{1}$$

Where $d$ is the aerodynamic diameter, ρ is the physical density, $\mu$ is viscosity, D is the characteristic dimensional scale of the physical system, and U is the characteristic velocity scale. Stokes' number can also be expressed as a ratio of the particle stop distance to dimensional scale of flow distortion (Vincent, 1994).

$$St = \frac{s}{D} \tag{2}$$

Stokes' number is a key scaling measure of an airborne particle's ability to respond to flow distortion. Small particles with corresponding small *St* values will be more likely to follow the changing flow trajectory. Larger particles on the other hand, will tend to follow the flow of their original motion (Vincent, 1994).

Particles of larger aerodynamic diameter are more susceptible to inertial and gravitational effects. For this reason, particle size selective inlets of thoracic and respirable cut points were considered. Proper inlet selection is crucial in the performance of the sampling system for efficient particle penetration. The following candidate inlets were selected for this research: 1) SKC single-stage inertial PM10 IMPACT sampler, 2) Tecora C.A.Th.I.A. and a 3) 3D printed Universal Inlet for Airborne-Particle Size-Selective Sampling.

**SKC IMPACT sampler**

The IMPACT Samplers from SKC Inc. (Figure 1) are single-stage inertial impactors that are designed to collect PM10, PM2.5, or PM Coarse (10-2.5). In the inertial impactor design theory, particles in the air enter the SKC IMPACT sampler through the inlet nozzles. Larger particles deviate from the airstream lines and impact on the impaction plate while smaller particles follow the airstream lines around the impaction plate and collect on the filter, Figure 2 (SKC Inc.).

In a validation study conducted by Trakumas and Salter (2009), the SKC IMPACT samplers were calibrated in the laboratory using an Aerodynamic Particle Sizer APS 3320 and indicated fair agreement with PM2.5 and PM10 particle size selective conventions as defined by EPA (1998).

Particles in the air enter the SKC IMPACT sampler through the eight 0.43 cm diameter inlet nozzles. The sampling efficiency curves of the PM10 IMPACT sampler is sharper than the PM10 curve defined by the EPA (Figure 3).

**Figure 1. IMPACT Sampler from SKC Inc. (SKC IMPACT sampler, 2016)**

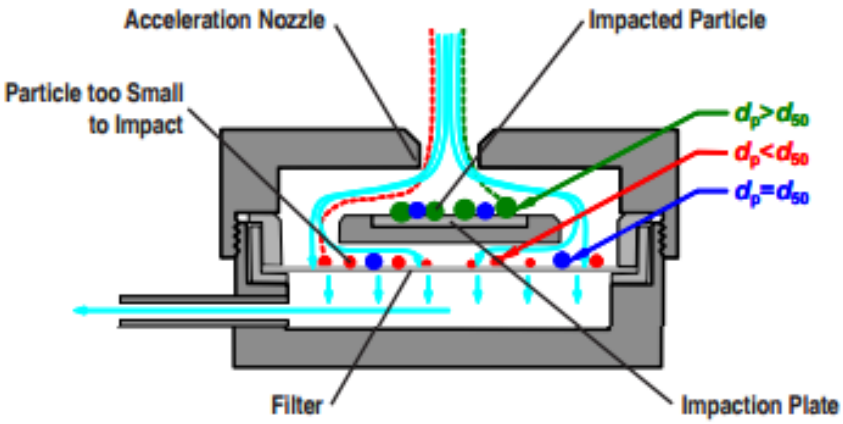


**Figure 2. Airstream Lines of IMPACT Sampler (Diagram courtesy of SKC, Inc.)**

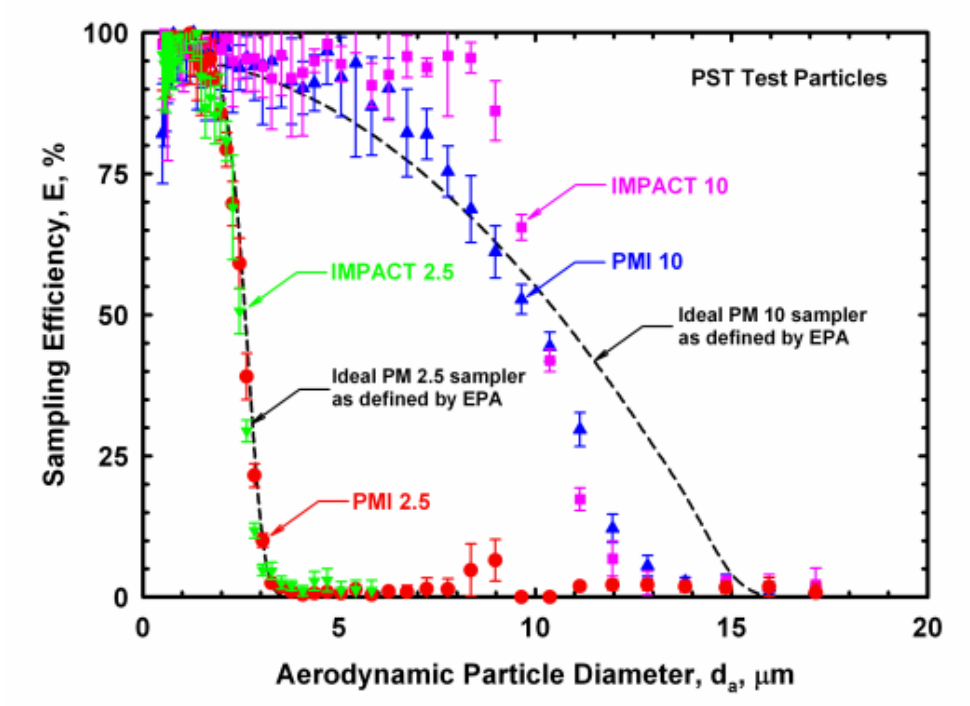


**Figure 3. Sampling Efficiency Curve for IMPACT sampler (Diagram courtesy of SKC, Inc.)**

**Tecora C.A.Th.I.A.**

The C.A.Th.I.A. developed by Tecora SLR is a modified version of the CIP-10, in Figure 4. This device utilizes omnidirectional aspiration for aerosol collection. The omnidirectional inlet protective cover blocks accidental, undesirable penetration of large particles or water drops. Instead of the rotating cup's rotations speed maintaining a constant flow rate as is used by the CIP-10, air is drawn through a pump to maintain the flow rate for collection. In a comparison of the thoracic CATHIA sampler with the standard cowled sampler from NIOSH 7400 standard method, Lee et al. (2008) concluded that the CATHIA has a "potential advantage as a high-flow static sampler for

screening coarse particles." In a study conducted by Jones et al. (2005), they found that the thoracic CATHIA has a slight oversampling for particles of aerodynamic diameter of 7 µm and less, however has selection characteristics similar to the thoracic convention.

Although the CATHIA sampler may not be appropriate as a personal sampler, its high flow rate and omnidirectional design makes it a possibly suitable inlet for mounting on a UAS sampling platform. Figure 5 depicts the airstream flow in the CATHIA inlet, Figure 6 shows the published efficiency curve for the CATHIA.

**Figure 4. C.A.Th.I.A Sampler from Tecora (Tecora C.A.Th.I.A, 2016)**

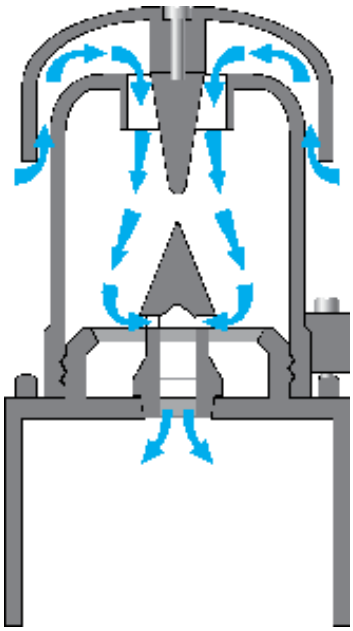

**Figure 5. CATHIA Airstream Flow (Diagram courtesy of Tecora, SLR)**

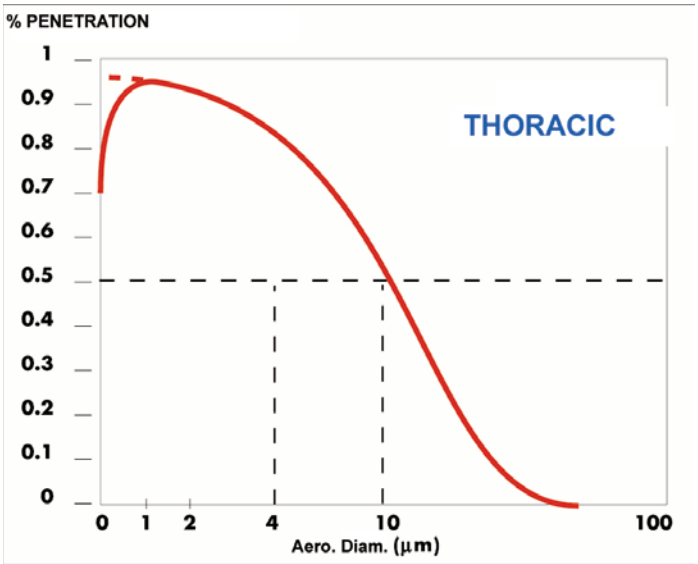


**Figure 6. CATHIA Efficiency Curve (Diagram courtesy of Tecora, SLR)**

**3D Printed Universal Inlet for Airborne-Particle Size-Selective Sampling**

In the patent for a Universal Inlet for Airborne-Particle Size-Selective Sampling invented by Raabe and Teague (1995), parallel jet orifices, collector holes, and stagnation chambers operate together as a size-selective airborne particle sampling device (Figure 7). This apparatus differs from impaction sampling because larger particles are collected in stagnation chambers preventing them from being re-entrained into the air stream. Collected particles do not interfere with the collection process because they are not in contact with the incoming air stream. The desired cut size requirements can be met by scaling the inlet or adjusting the airflow. The basic principles of this patent design were developed using SolidWorks software and produced with a ProJet 3500 Max three-dimensional printer. More in-depth design and analysis parameters will be discussed in Chapter 5.

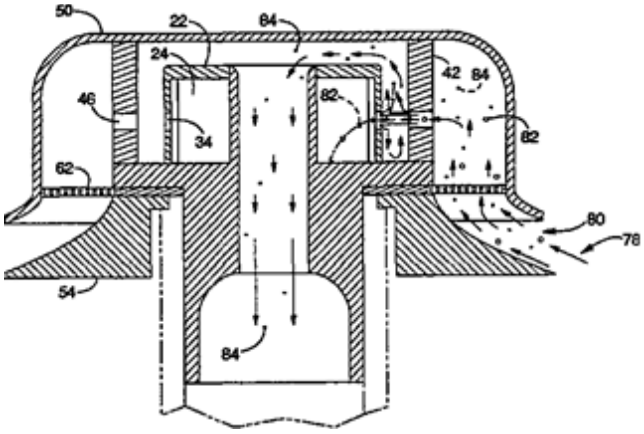


**Figure 7. Universal Inlet For Airborne-Particle Size-Selective Sampling by Raabe et al. (Raabe & Teague, 1995)**

## Bluff bodies

Bluff bodies in an airstream are subject to a blockage constraint because the boundaries of the walls prevent a free lateral displacement of the airflow (Maskell, 1965). Bluff bodies are characterized by a separation of the boundary layer from their surface and a high coefficient of drag (Buresti, 2000). A blockage constraint is the flow past a body in an airstream that is higher than in an unlimited stream because the proximity of a solid wall and can cause an acceleration of the airflow as it deviates past a body (Maskell, 1965 & Vincent, 2007). Detailed model simulations suggest that blockage ratios up to 15% have limited impact on the properties in the wind tunnel (Anagnostopoulos et al., 1996). Often a blockage ratio of 10% is recommended for wind tunnel studies; however, 30% blockage is considered satisfactory for aerosol sampler research (Vincent, 2007). Just as sampling efficiency of personal aerosol samplers is influenced by the body of the operator (Gorner, 2009) it is expected that the selected inlets will also be influenced by the UAS platform.

## Thoracic and Respirable Particle Penetration

The concept of size-selective particle sampling has been employed as a means for effectively sampling the particle sizes associated with specific pathologic outcomes. The regional pattern of particle deposition in the respiratory tract affects the pathogenic potential of inhaled aerosols (Brown et al., 2013). Sampling the total air concentration of particulate matter (PM) allows a crude estimate of exposure that may not correlate with observed health effects if the risk is associated only with those particles that may enter

the thorax or penetrate beyond the ciliated airways (Brown et al., 2013). Brown et al. defines the size selective fractions as follows:

- Inhalable fraction – the mass fraction of total airborne particles which is inhaled through the nose and mouth.
- Extrathoracic fraction – the mass fraction of inhaled particles failing to penetrate beyond the larynx.
- Thoracic fraction – the mass fraction of inhaled particles penetrating beyond the larynx.
- Respirable fraction – the mass fraction of inhaled particles penetrating to the unciliated airways.

**Conclusion**

To advance the capabilities of aerosol monitoring in occupational hygiene practices, combining the technology of multi-rotor unmanned aerial systems with aerosol sampling devices needs to continue to be explored. The evolving technology of unmanned aerial systems offers a capability for remote sensing and emission monitoring at favorable precision and accuracy levels. This will allow for the ability for repeatable fine-scale projects in air quality monitoring without resorting to additional worker hazard exposure and preventing the requirement for site visits (Watts et al., 2012). The advancing UAS technology will be beneficial in the applications of occupational hygiene monitoring. Industrial workers, the community, and occupational hygienist are exposed to a wide range of hazards, including but limited to particulate matter, heavy metals, polycyclic aromatic hydrocarbons, and volatile organic chemicals. By utilizing a small

multi-rotor UAS in aerosol sampling and monitoring, tasks can be accomplished remotely and effectively while limiting hazard exposure.

**Summary**

In the study conducted by Chang et al., contaminant emission sampling was performed to demonstrate the applicability of the multi-rotor-carried air sampling apparatus with agile maneuverability and precision. Studies similar to the one conducted by Chang et al., Brady et al., and Altstädter et al. are most closely related to the future plans of UAS carrying aerosol sampling devices and sensors. The capabilities of UAS as a sampling platform need to be further investigated to enhance versatility in applications of occupational hygiene. Some of the gaps in research and potential future studies for aerial whole air sampling outlined by Eninger and Johnson include:

> Particle sampling design valid sampling methods across varied flight profiles; facilitate isokinetic/particle-size selective sampling; modeling via computational fluid dynamics; laboratory and field testing; chemical sensors and software algorithms to follow or map contaminant concentration gradients and locate or characterize contaminant sources autonomously. (Eninger & Johnson, 2015)

The purpose of this research will be to contribute to the understanding of aerosol sampling and collection using a contemporary multi-rotor UAS as a sampling platform.

# III. Methodology

## Chapter Overview/Introduction:

Unmanned Aircraft Systems (UAS), unmanned aerial vehicles (UAVs), and remotely piloted aircraft (RPA), have a contributing history in their support of military warfare efforts. Unmanned aerial systems (UAS) have the potential to serve as mobile platforms for environmental monitoring. A gap in the literature exists in the area of aerosol sampling and collection using multi-rotor UAS as a sampling platform. The objective of this research was to close the gap in the area of aerosol sampling and collection using contemporary multi-rotor UAS as a sampling platform. Optimal configurations for aerosol particle collection on a multi-rotor, small UAS were determined. This chapter outlines the experimental method utilized for determining the sampling efficiencies of selected aerosol inlets mounted on an unmanned aerial system.

## Applicability of UAS as a Sampling Platform

Fixed wing unmanned aircraft are more suitable for extended flight time over a long distance, while multi-rotors (i.e. quad-rotors) are more practical for smaller mapping areas or the need for stationary monitoring (Harriman and Muhlhausen, 2013). Investigations of aerosol sampling on fixed-wing UAS were conducted in studies by Watts et al., Craft et al., and Corrigan et al. The placement of aerosol inlets and sensors on forward flight UAS were studied by Bernard and Krispin (2010) and Hermann et al. (2001) to minimized the influence of the aircraft on the sample aerosol.

The characterization of vertical profile measurements of aerosol parameters is integral in understanding the contributions of heating/cooling in differing atmospheric layers because surface and remote measurements do not always accurately reflect aerosol behavior (Corrigan et al., 2008). The utilization of UAS in engineering and environmental industries and its abilities in contamination monitoring continue to be characterized by researchers. In a study conducted by Chang et al., a multi-rotor UAS was designed with the air sampling techniques of an evacuated canister to demonstrate its field applicability (2015). The study deployed a field mission of the multi-rotor hovering over an exhaust shaft of a roadway tunnel to collect air samples carrying a lightweight remote-controlled whole air sampling component. The major advantages resulting from the study demonstrated: 1. the maneuverability of the multi-rotor coupled with the aerosol sampler can be readily deployed for environmental studies; 2. Aerial sampling and preservation conditions can be performed at desired positions; and 3. Data for a large array of vertical profiles of gaseous species can be easily obtained (Chang et al., 2015).

**Small Unmanned Aerial System**

The small UAS used in this research was designed and built by the AFIT ANT Center (Figure 8). The UAS has an eight motor configuration, and weighs approximately 8 kg with the battery included.

The components of the UAS included:

- KDE Direct 75A+HV electronic speed controller (ESC) – The ESC includes an all-Aluminum 6061-T6 case

- Eight KDE Direct 5212XF-330 Multi-Rotor Brushless Motors – includes 200°C, 760mm silicone-wire leads and ϕ4.0mm 24k Bullet Connectors
- 960 mm Tarot X Quad frame
    - Specifications :

      Motor to Motor spacing : 960 mm

      Propeller standard : 56~61 cm

      Arm lengths: 392 mm

      Arm diameter: 25 mm

      Arm weight : 113 g

      Main frame diameter: 330 mm

      Ground clearance: 320 mm (Rail to ground)

      Battery standard: 22.2V (6S), 10000-20000 mah
- Autopilot: Pixhawk running Ardupilot firmware

Observational flight tests conducted by the ANT Center concluded an expected average flying time of 20-25 mins. The UAS was certified for airworthiness in accordance with the Federal Aviation Administration guidelines.

**Figure 8. Photograph of Multi-rotor UAS with CATHIA Mounted**

**Procedures and Processes**

Three experiments were conducted to meet the specific aims introduced in Chapter 1. These experiments included: 1) airflow visualization, 2) particle sampling efficiency comparison of inlets at varying orientations and while mounted on a UAS in the University of Cincinnati aerosol test chamber, 3) particle sampling efficiency comparisons of inlets while mounted on a UAS in the West Virginia University wind tunnel. Airflow visualization on the multi-rotor UAS was conducted in the NIOSH Cincinnati, Ohio tracer gas room, in conjunction with a fog generator and horizontal and vertical plane lasers. Results from the airflow visualization determined the optimal placement for the selected air sampling inlets. The three candidate inlets to investigate

the applicability of aerosol sampling on a multi-rotor unmanned aerial systems (UAS) included: a single-stage inertial SKC IMPACT sampler from SKC, C.A.Th.I.A. by Tecora SLR, and a 3-D printed *Universal Inlet for Airborne-Particle Size-Selective Sampling* based on the design of Raabe et al. (Raabe & Teague, 1995). These inlets were selected based on their particle size selectivity, omnidirectional operation, and potential functional independence to wind speed and direction, and were designed for 50% cutpoints of 10 µm aerodynamic diameter at the manufactured recommended sampling flow rates of 10, 7, and 10 LPM respectively.

Typical workplace ambient air velocities are considered calm or low moving air and range from 1 – 4 m/s (Baron, 2016). Optimal weather conditions for flying UAS are on sunny days with little to no wind. The National Oceanic and Atmospheric Administration define a calm to light air as wind speeds of < 0.3 – 1.5 m/s. Tests were repeated at 0 and 0.254 m/s cross-sectional airflow to reflect typical workplace conditions and optimal UAS flying weather conditions. An experimental method was designed to compare the sampling efficiencies of these inlets in still-air environment and the effects when mounted on the UAS sampling platform.

**Experiment 1: Airflow Visualization.**

In a study conducted by Huang et al. (2015), flow simulations were conducted on a quadrotor UAS in hovering and forward flight. Their investigation of the aerodynamic interaction between rotors and fuselage found that strong downwash flow is induced by the tip vortices. They also observed a slightly higher downward velocity distribution around the fuselage (Hwang et al, 2015). Observations such as those found by Hwang et

al. are key in aerosol inlet placement considerations. Although complex computational fluid dynamics studies were not conducted on the multi-rotor utilized in our study, airflow visualization was performed on the UAS to determine an optimal inlet mounting location.

Experiment 1 was conducted to address Specific Aim 1 in the tracer gas room of the Division of Applied Research and Technology, National Institute for Occupational Safety and Health in Cincinnati, Ohio. The tracer gas test chamber was utilized to conduct airflow visualization on the multi-rotor UAS. The UAS was placed in the center of the tracer gas side and mounted on a small table. Cables strapped the UAS legs to the table with two 80 lb weights at the bottom of the straps to keep the UAS in place. Three GoPro Hero 3 White Edition cameras, and one Sony 4K video camera were mounted on Magnus VT-300 tripods and situated around the UAS. One vertical laser was set diagonally across the room and one horizontal laser set above the top UAS propellers with a maximum power output of < 5 MW and a wavelength of 532 nm. Fog was generated directly in front of the UAS with a Chauvet Hurricane 1100 with DegreeC airflow visualization fluid, ultra grade, specialized formula, propylene glycol. A schematic of the tracer gas room is depicted in Figure 9 and picture of the setup from the observation room side in Figure 10. With the lights in both the Observation Room Side and Tracer Gas Side off, enough fog was generated to cover all eight motors and propellers of the UAS. Once enough fog was generated, the UAS was powered at 50% of its thrust capacity. This thrust setting simulated hovering and forward flight of the UAS without causing unwanted stress on the strapped down legs.

Airflow velocity above and below the UAS fuselage was measured using a TSI VelociCalc. The airflow velocities 22 cm above and 13 cm below the fuselage of the UAS, and 14 cm underneath a propeller were measured.

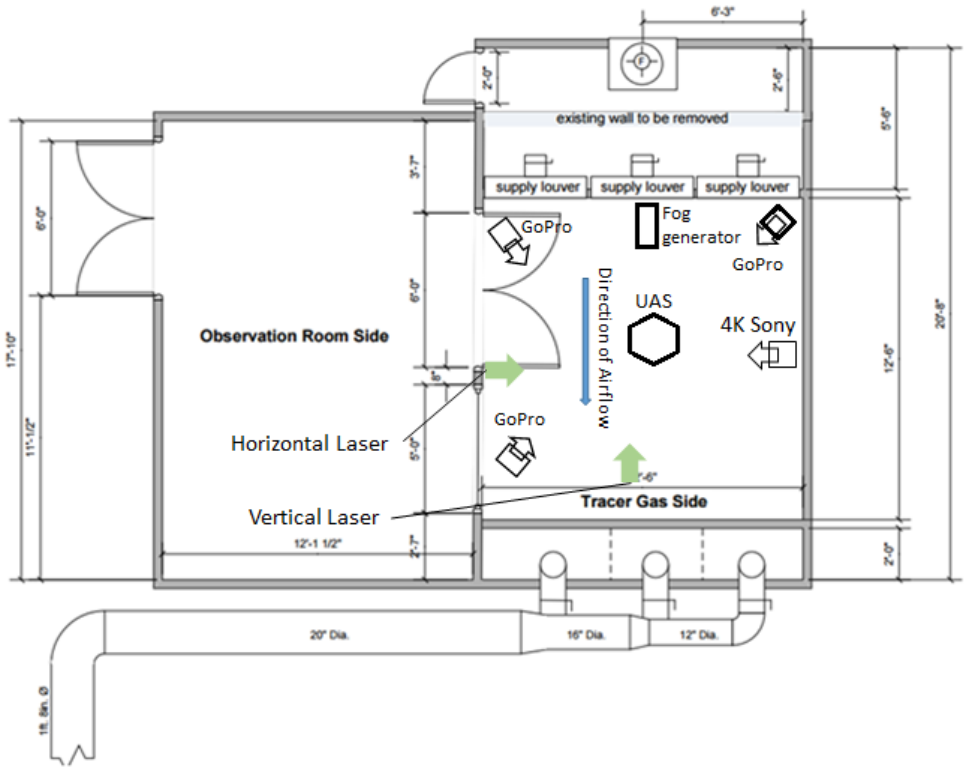


**Figure 9. NIOSH Tracer Gas Room Diagram of UAS Airflow Visualization Setup – Planar View (Modified diagram courtesy of NIOSH Division of Applied Research and Technology)**

**Figure 10. Airflow Visualization Setup**

**Experiment 2: Inlet Characterization in Still-Air University of Cincinnati Aerosol Test Chamber**

The selected inlets were first characterized in an aerosol test chamber set at 0 m/s wind speed to gain knowledge of their limitations and capabilities to address specific aim 2. Experimental tests were conducted in the walk-in chamber at the University of Cincinnati (UC). The chamber is 24 $m^3$ and located in the Center for Health Related Aerosol Studies, with the built-in ventilation system turned off. The same chamber was described in the study conducted by Peck et al. (2015).

**Test Aerosol**

Several test aerosols were considered for this research (ie. Polystyrene latex (PSL) spheres, Arizona Road Dust, NaCl, KCl, and sugar). Monodisperse test aerosols of polystyrene latex (PSL) spheres of 2, 4, 10 µm aerodynamic diameter were considered. Although more detailed and accurate studies can be conducted, the use of monodisperse aerosol of known particle size can be costly and requires time-consuming test repetitions (John and Kreisberg, 1999). Polydisperse Arizona Road Dust (ARD) 5 which has a nominal aerodynamic diameter ranging between 0.5 to 10 µm were generated and introduced into the test chamber.

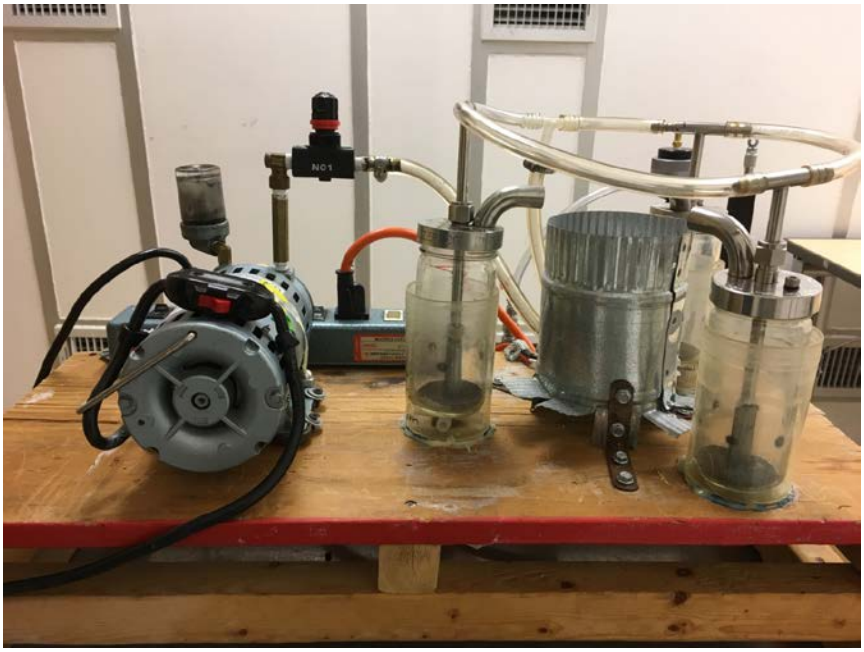

**Figure 11. Aerosol Generator with Three Nebulizers**

The test aerosol was generated with an air pump producing 12.5 LPM of air into three 6-jet Collison Nebulizers (BGI Inc., Waltham, MA, USA) containing the ARD 5

(Figure 11). The test aerosol was not charged neutralized and was drawn from the atomizer vessels and a high-velocity air flow broke up the sonicated powder suspending the aerosol. A small horizontal fan suspended the aerosol, while an offset vertical fan dispersed the aerosol in the direction of the inlet. This aerosol generation method was similar to experimental set up in the study conducted by Peck et al. (Peck et al. 2015). The concentration of aerosols in the chamber was determined by a GRIMM 1.108 portable aerosol counter, and was measured between sample collections to ensure uniformity.

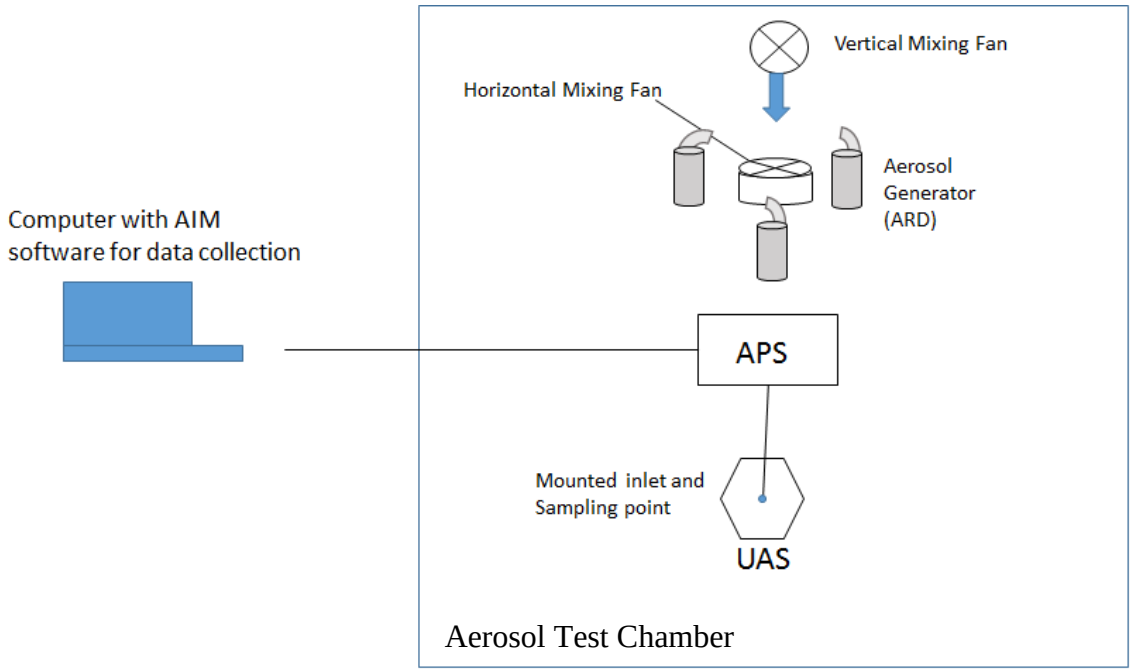


**Figure 12. Test Setup of UAS On vs. Off Comparisons – Planar View**

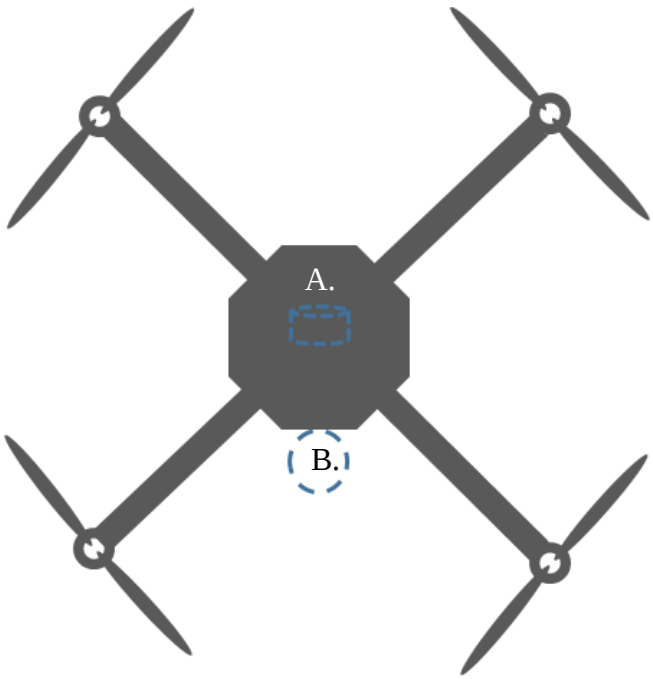


**Figure 13. Planar View of Aerosol Inlet Mounting Location on UAS, A. SKC PM10 IMPACT Location, B. 3D Printed Inlet and CATHIA Location (Not to scale)**

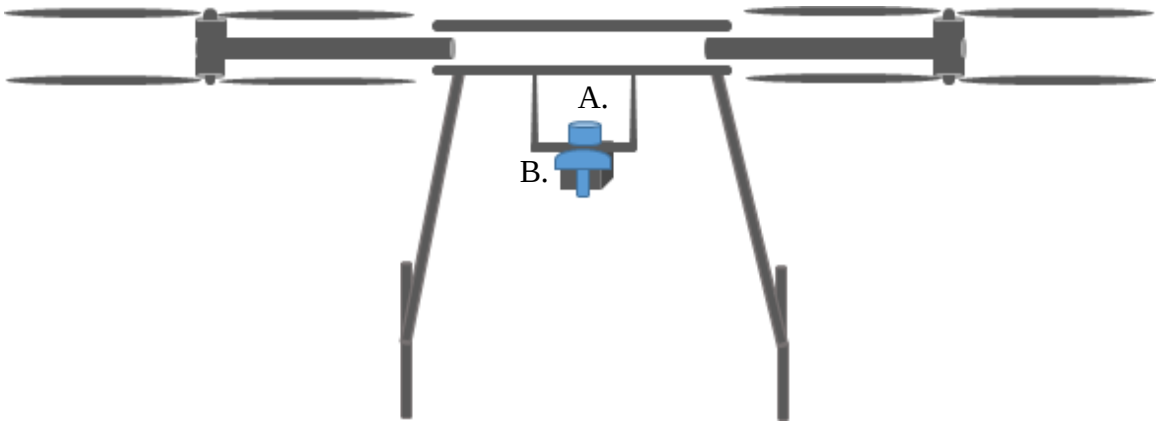


**Figure 14. Elevated View of Aerosol Inlet Mounting Location on UAS, A. SKC PM10 IMPACT Location, B. 3D Printed Inlet and CATHIA Location (Not to scale)**

**Sample Collection**

An aerodynamic particle sizer was used to determine particle count and size distributions in real time (Kesavan and Bottiger, 2005) while data was recorded on a computer situated outside of the aerosol chamber. The test set-up of experiment 2 are depicted in Figure 12, and the placement of the mounted candidate inlets are depicted in figures 13 and 14. The exiting nozzle of the size-selective inlets were connected to an aerodynamic particle sizer. A flow divider directed flow toward both the APS analyzer and to an A.P Buck Libra Plus LP-20 high flow pump. Flow rates through each air sampling inlet were determined by pre and post calibration using a TSI 4000 Series Model 4045 G mass flowmeter. The IMPACT sampler was calibrated with the SKC calibration adapter, while the 3D printed inlet and CATHIA were calibrated with modified air tight calibration jars. Measurements of the aerosol and particle size transmitted through the sampler inlets were verified by an APS to compare the mean count concentrations and variances between the candidate inlets at varying orientations and while mounted on the UAS.

Orientation comparisons were conducted while mounted on a tripod in the upright, upsidedown, and horizontal (forward facing the aerosol generator) directions for each candidate inlet. The APS was set to record data in 20 second increments, and sampled for 2 mins at each orientation. Sampling collection was repeated in triplicate for every inlet, resulting in an N of 18 samples at every orientation (a total N of 54 for all three orientations).

Particle sampling efficiencies of the candidate inlets were also compared in a mounted arrangement on the UAS with and without rotor employment. Samples were recorded from the APS for 20 seconds at a 2 min duration alternated in quadruplicate between UAS rotor on and off, resulting in an N of 24 for each rotor employment scenario (a total N of 48 for each inlet).

**Experiment 3: Inlet Characterization in West Virginia University Wind Tunnel**

**Wind Tunnel**

To address specific aim 3, additional tests in the West Virginia University (WVU) wind tunnel were conducted to investigate the effects in a calm to light air moving environment. The second test chamber was a 3.6 x 2.7 x 12 $m^3$ wind tunnel laboratory at WVU (Figure 15). The wind tunnel was equipped with three separate chambers: mixing, experimental, and plenum. The test set-up was conducted in the experimental chamber of the wind tunnel (Figure 16). Airflow through the wind tunnel was set at 0.254 m/s and induced with a type BCV-SW large-capacity industrial fan (Twin City Fan Companies Ltd., Minneapolis MN) and operated with a Baldor Series 15-H Inverter and digital control (Lewis, 2010). A handheld TSI Condensation Particle Counter 3007 was used to ensure aerosol generation uniformity in the West Virginia University wind tunnel.

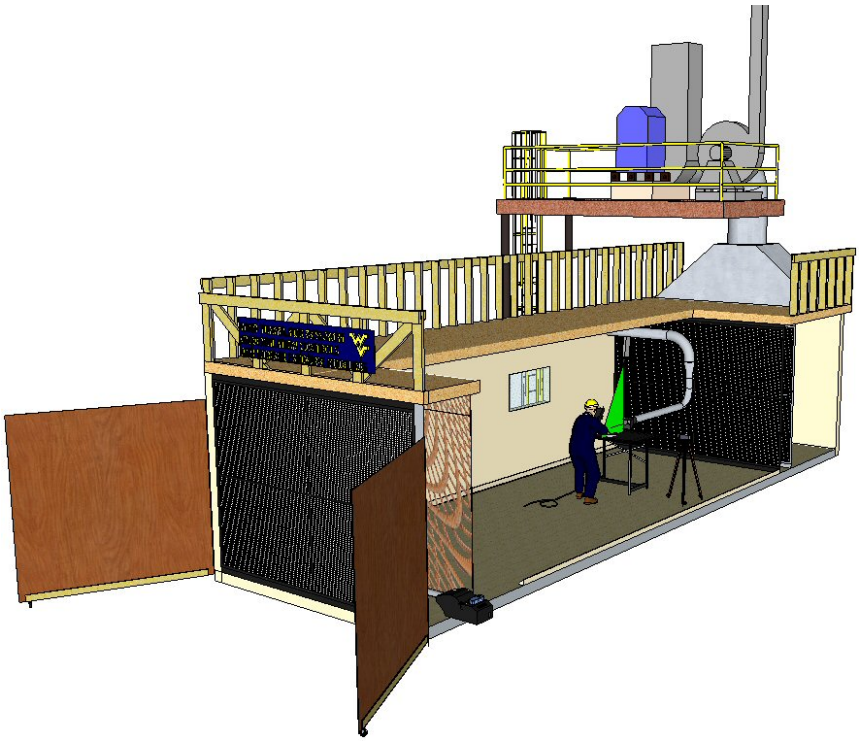

**Figure 15. West Virginia University Wind Tunnel (Diagram courtesy of Industrial & Management Systems Engineering West Virginia University)**

**Test Aerosol**

The test aerosol used in the WVU wind tunnel was not charged neutralized and was generated by a TSI six-jet atomizer from a 0.2 g/mL sugar solution. The atomizer was situated on the ground, 1.2 m upwind of the UAS. All six jets of the atomizer were employed, and pressure was set at a 35 psi with 20 LPM dilution air.

**Sample Collection**

Just as sample collection in the UC aerosol test chamber, particle sampling efficiencies of the candidate inlets were compared with and without rotor employment

while mounted on the UAS. Data was recorded from the APS for 20 seconds at a 3.33 min duration alternated in triplicate between UAS rotor on and off, resulting in an N of 33 (a total N of 66 for each inlet). A summary of the test conditions for experiments 2 and 3 are outlined in Table 1.

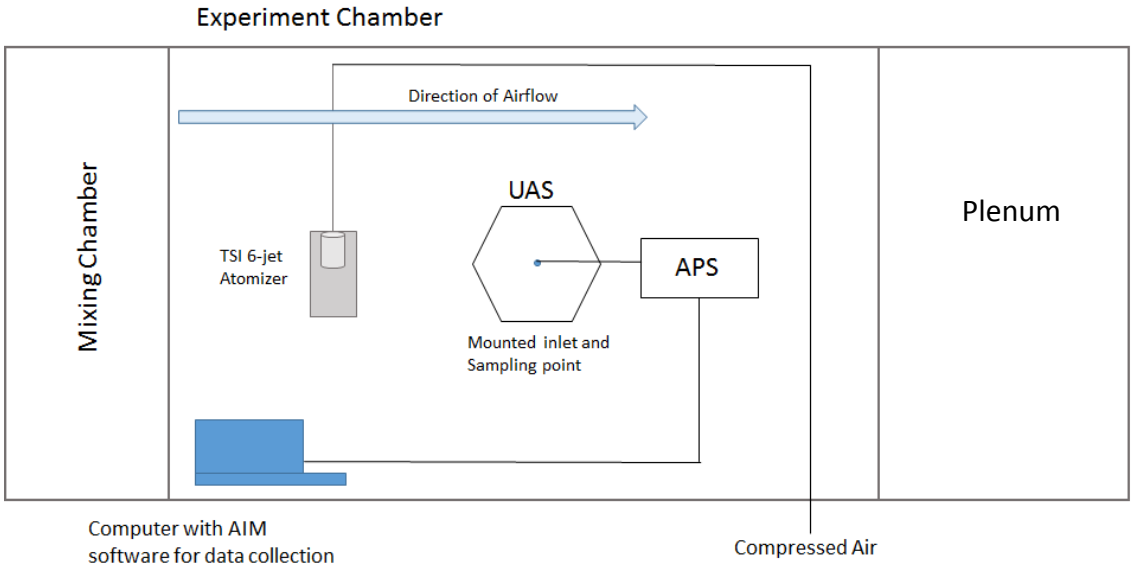


**Figure 16. Test Setup of UAS On vs. Off Comparisons in WVU Wind Tunnel – Planar View (Not to scale)**

## Interpretation of Results

Just as sampling efficiency of personal aerosol samplers is influenced by the body of the operator (Gorner, 2009) it was expected that the sampling efficiency of the selected inlets would also be influenced by the UAS platform. Airflow visualization of the UAS was conducted to determine feasible locations on the UAS with minimal bias to mount the sampling inlets. Sampling bias determination for UAS airframe and aerosol sampler

in hovering and forward flight was derived from comparative statistics on the mean particle counts, by particle size bin. The measures of variability were compared between rotor on and off conditions by Analysis of Variance (ANOVA) and Tukey means difference tests.

To test for normal distribution, the Shapiro-Wilk Test was conducted on the distribution of particle count from the GRIMM read-out display.

The tested hypothesis for normality:

$H_0$: Particle counts are normally distributed between sampling collections

$H_a$: Particle counts are not normally distributed between sampling collections

Analysis of Variance of the varying inlet orientations and variable parameters of the UAS on versus off was conducted in order to determine if there were statistically significant differences. To find statistical significance using ANOVA the distribution of data was determined to represent a normal distribution. A Tukey means difference test was conducted to determine the statistical differences among inlet orientations. To test for constant variances, a Levene test was conducted. When the Levene test failed against an alpha of 0.05, a Welch's test was conducted. The null hypothesis $H_O$ where all the variances are equal was tested with the alternative hypothesis $H_a$ that at least one of the orientations variances differs.

The tested hypothesis for equal means:

$H_0$: $\mu_1 = \mu_2 = \mu_3$ (where $\mu_i$ represents the true mean particle count for inlet orientation and UAS on vs. off)

$H_a$: At least one of the particle count means differ

The tested hypothesis for equal means in the effect test:

$H_0$: $\mu_1 = \mu_2 = \mu_3 = \mu_4$ (where $\mu_i$ represents the true mean for orientation or UAS parameter *i*)

$H_a$: At least one of the particle count means differ

The tested hypothesis for equal variances:

$H_0$: $\sigma^2_1 = \sigma^2_2 = \sigma^2_3 = \sigma^2_4$ (where $\sigma^2_i$ represents the variance for inlet *i*)

$H_a$: At least one of the orientation variances differ

Each tested hypothesis was conducted for 42 aerodynamic diameter bin sizes of 0.542 – 10.366 µm with ARD as the test aerosol, and 33 bins 0.542 – 5.425 µm for sugar test aerosol. P-values were determined for each aerodynamic bin size and were then combined as a single statistic determined using Fisher's Method:

$$-\mathbf{2}\sum_{i=1}^{k}\mathbf{ln}(\boldsymbol{p_i}) \tag{3}$$

Where $p_i$ is the representative independent p-value, and *k* is the number of p-values to be combined.

Percent differences between aerosol sampling concentrations when the UAS was on vs. off were also conducted:

$$\frac{\textit{Concentration with UAS ON} - \textit{Concentration with UAS OFF}}{\left(\frac{\textit{Concentration with UAS ON} + \textit{Concentration with UAS OFF}}{2}\right)} \times \mathbf{100}\% \tag{4}$$

**Table 1. Test Condition Summary for Experiment 2 and 3**

| Test Condition | Test Aerosol | Aerodynamic Diameter (µm) | Aerosol Sampler | Sampler Orientation | Test Location | Air Velocity | Mounting Arrangement | UAS On/Off | N |
|---|---|---|---|---|---|---|---|---|---|
| 1 | ARD | 0.5 - 10 | IMPACT | Upright | UC | Still | Tripod | N/A | 18 |
| 2 | ARD | 0.5 - 10 | IMPACT | Upside down | UC | Still | Tripod | N/A | 18 |
| 3 | ARD | 0.5 - 10 | IMPACT | Horizontal | UC | Still | Tripod | N/A | 18 |
| 4 | ARD | 0.5 - 10 | CATHIA | Upright | UC | Still | Tripod | N/A | 18 |
| 5 | ARD | 0.5 - 10 | CATHIA | Upside down | UC | Still | Tripod | N/A | 18 |
| 6 | ARD | 0.5 - 10 | CATHIA | Horizontal | UC | Still | Tripod | N/A | 18 |
| 7 | ARD | 0.5 - 10 | 3D Printed | Upright | UC | Still | Tripod | N/A | 18 |
| 8 | ARD | 0.5 - 10 | 3D Printed | Upside down | UC | Still | Tripod | N/A | 18 |
| 9 | ARD | 0.5 - 10 | 3D Printed | Horizontal | UC | Still | Tripod | N/A | 18 |
| 10 | ARD | 0.5 - 10 | IMPACT | Upright | UC | Still | UAS | Off | 24 |
| 11 | ARD | 0.5 - 10 | IMPACT | Upright | UC | Still | UAS | On | 24 |
| 12 | ARD | 0.5 - 10 | CATHIA | Horizontal | UC | Still | UAS | Off | 24 |
| 13 | ARD | 0.5 - 10 | CATHIA | Horizontal | UC | Still | UAS | On | 24 |
| 14 | ARD | 0.5 - 10 | 3D Printed | Upright | UC | Still | UAS | Off | 24 |
| 15 | ARD | 0.5 - 10 | 3D Printed | Upright | UC | Still | UAS | On | 24 |
| 16 | Sugar | 0.5 - 5 | IMPACT | Upright | WVU | 0.254 m/s | UAS | Off | 33 |
| 17 | Sugar | 0.5 - 5 | IMPACT | Upright | WVU | 0.254 m/s | UAS | On | 33 |
| 18 | Sugar | 0.5 - 5 | CATHIA | Horizontal | WVU | 0.254 m/s | UAS | Off | 33 |
| 19 | Sugar | 0.5 - 5 | CATHIA | Horizontal | WVU | 0.254 m/s | UAS | On | 33 |
| 20 | Sugar | 0.5 - 5 | 3D Printed | Upright | WVU | 0.254 m/s | UAS | Off | 33 |
| 21 | Sugar | 0.5 - 5 | 3D Printed | Upright | WVU | 0.254 m/s | UAS | On | 33 |

# IV. Results

## Airflow Visualization

Airflow visualization was performed on the UAS to determine an optimal inlet mounting location. Lasers were situated in both the vertical and horizontal planes to determine airflow visualization around the multi-rotor UAS. Fog was generated to cover all eight propellers before powering the UAS. From Figures Figure 17 –Figure 20, the top propellers pulled the generated smoke, clouding the top carriage of the main body with fog. Figure 21 displays the airflow movement with the propellers employed, with an overlay of the instantaneous vertical downward velocity contours from the study conducted by Hwang et al. (2015). After about 6 seconds of UAS power, the fog was completely mixed in the chamber (Figure 22). The airflow velocity measured 22 cm above the fuselage resulted in a flow rate of 2.2 m/s, while 13 cm below the fuselage resulted in an average flow rate of 0.92 m/s. The numerical and visual results concluded that directly below the fuselage of the UAS was optimal placement for an air sampling inlet. The size of the aerosol sampling inlets limited the mounting placement under the fuselage of the UAS. The SKC IMPACT sampler was the only inlet small enough to fit directly center of the mounting plate. The 3D printed inlet was strapped to the battery just at the edge of the mounting plate. Because of the length and weight of the CATHIA, it was forced to be mounted in a horizontal orientation on the plate.

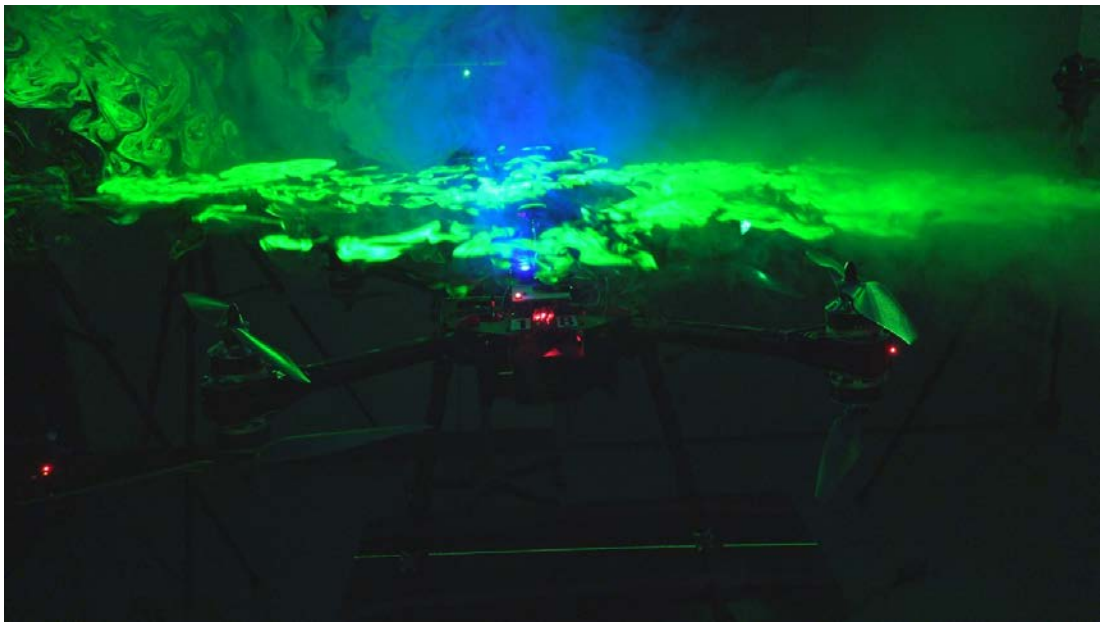

**Figure 17. Beginning of Fog Generation with Propellers Off**

**Figure 18. Initial Airflow Movement with Propellers On**

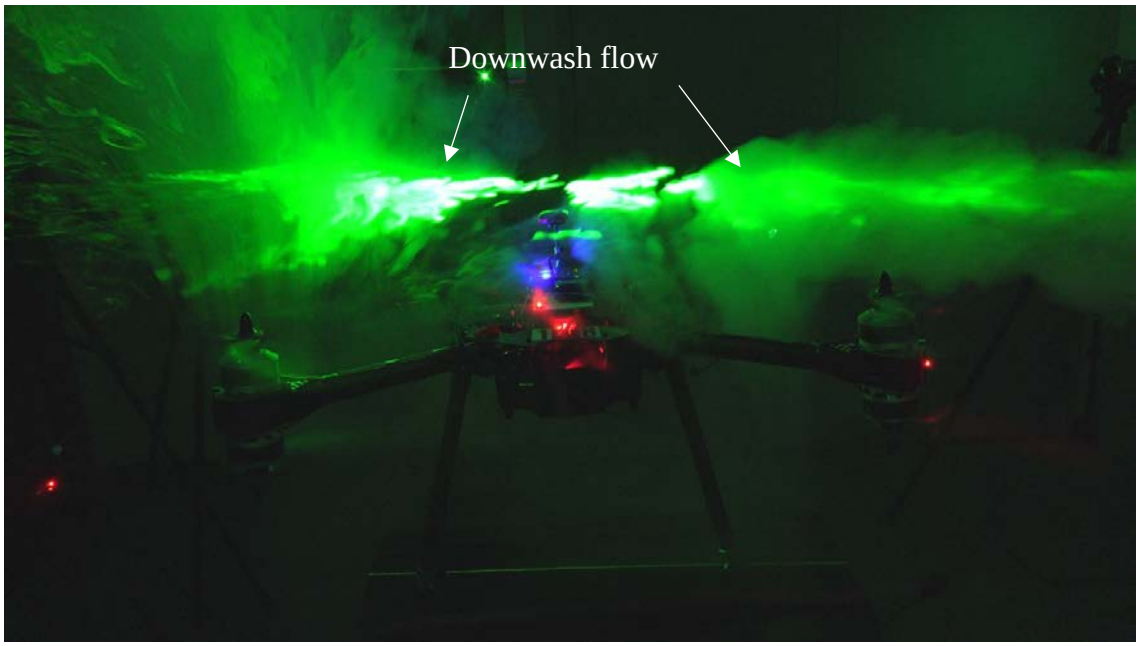


**Figure 19. Airflow Movement after 1.02 seconds with Propellers On**

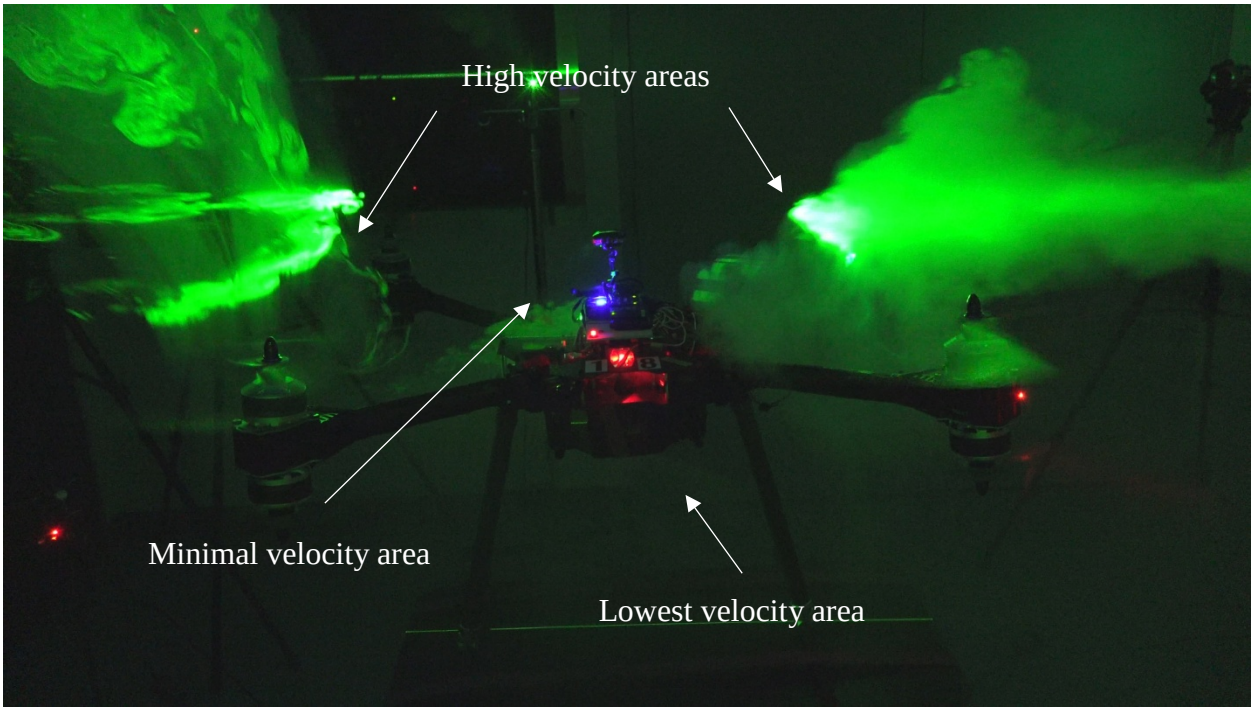


**Figure 20. Airflow Movement after 2.02 seconds with Propellers On**

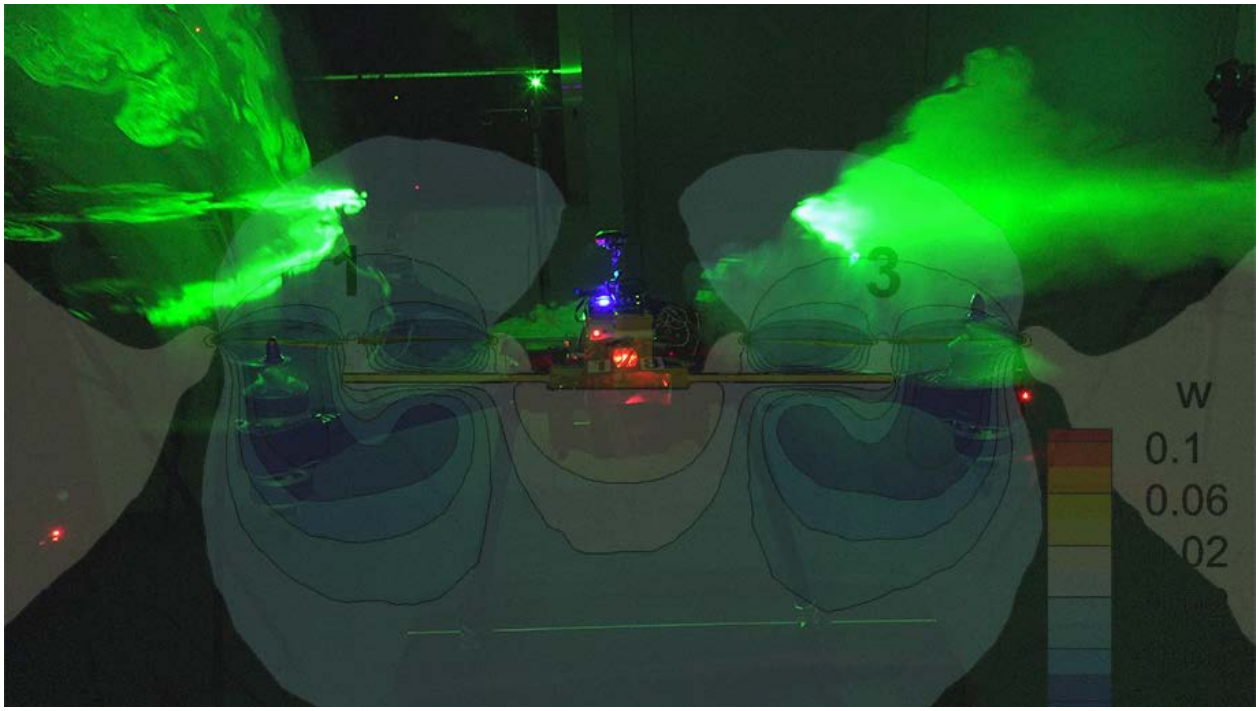


**Figure 21. Airflow Movement after 2.02 seconds with Overlay of Instantaneous Vertical Downward Velocity Contours (Overlay image modified from Hwang et al., 2015)**

**Figure 22. Complete Mixing after 6.06 seconds with Propellers On**

**Aerosol Chamber Concentration Distribution**

Uniformity of the ARD generated in the University of Cincinnati aerosol chamber was measured with the GRIMM. The summary statistics of the plotted concentration throughout aerosol sampling tests resulted in a mean concentration of 6657±103 #/cm$^3$ for particles 2 µm and larger (Figure 23). The histogram plot and Shapiro-Wilk test showed statistical significance of normality (Figure 24). The P-Value of 0.9166 is greater than the alpha of 0.05, therefore fails to reject the null hypothesis that the data is from a normal distribution.

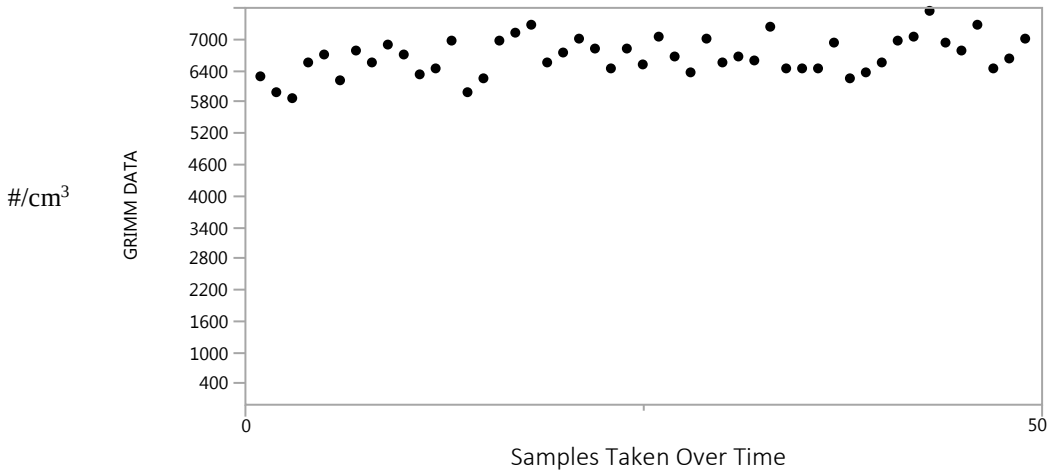


**Figure 23. Overlay Plot of Aerosol Concentration in UC Chamber with GRIMM**

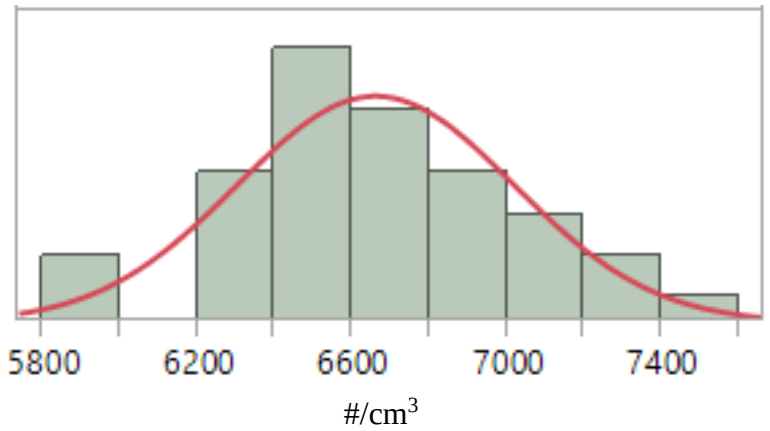


**Figure 24. Histogram Plot of Aerosol Concentration in UC Chamber with GRIMM**

Aerosol generation uniformity in the West Virginia University wind tunnel was measured with a Condensation Particle Counter with glucose solution as the test aerosol (Figure 25), and resulted in a mean concentration of 14783±217 #/cm$^3$. The Shapiro-Wilk test showed no statistical significance of normality. The P-value of < 0.0001 is less than the alpha of 0.05, therefore, Shapiro-Wilk rejects the null hypothesis and determines the distribution is not normally distributed. However, the near normal curve displayed

within the Histogram is an allowable violation as the data appears to fit a normal distribution (Figure 26).

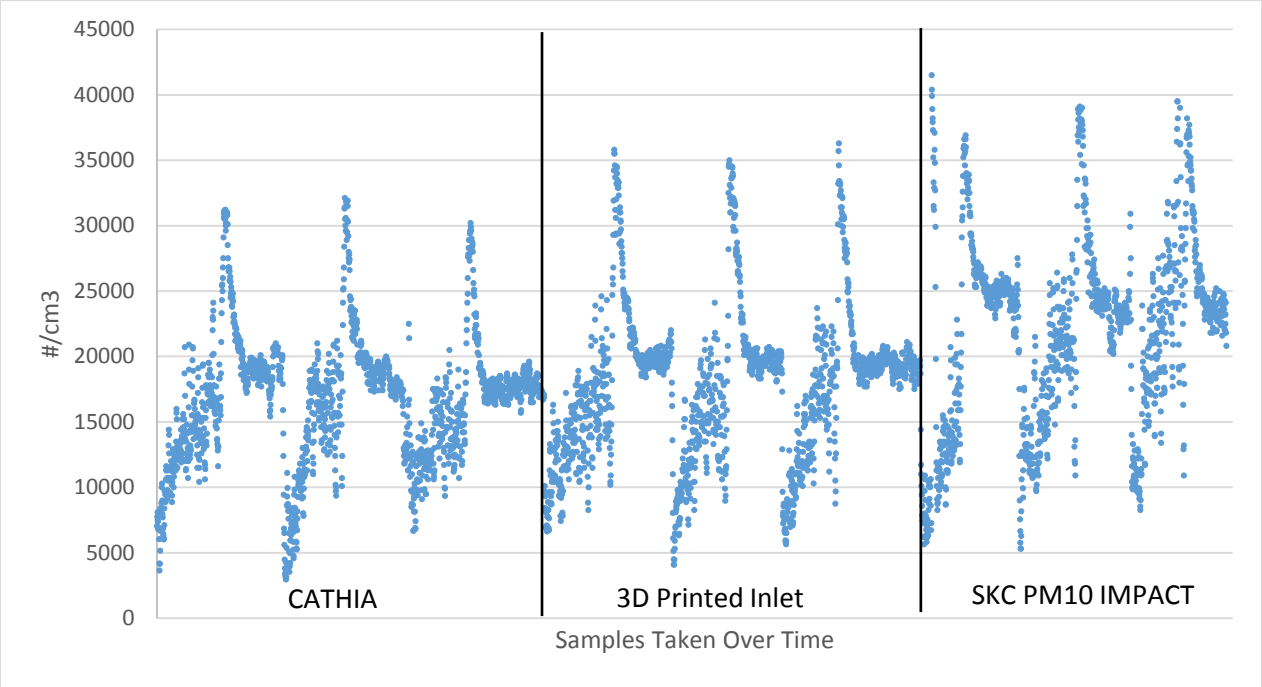


**Figure 25. Particle Count Concentration from CPC Taken Over Time in WVU Wind Tunnel**

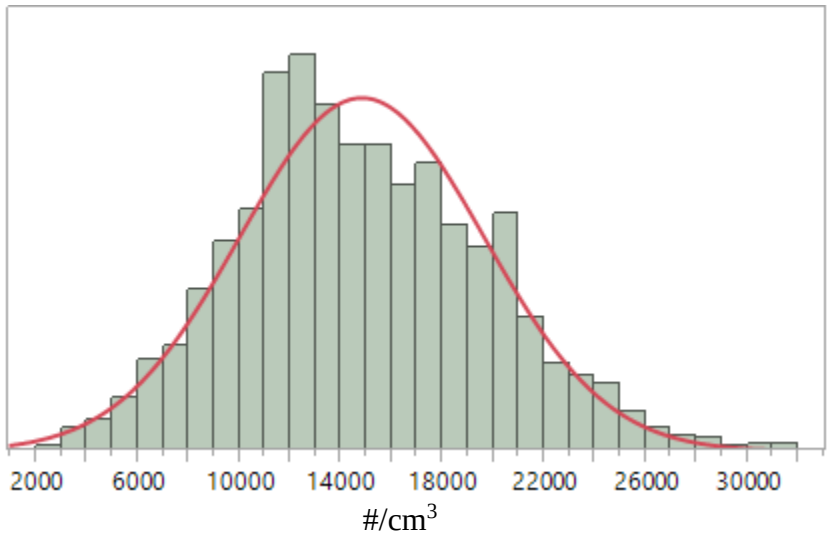


**Figure 26. Histogram Plot of Aerosol Concentration in WVU Chamber with CPC**

**Aerosol Inlet Orientations**

Once the placement of the aerosol inlet on the UAS was determined, varying orientations of each candidate inlet were considered for mounting. While mounted on a tripod, each inlet was tested in the upright, upside down, and horizontal (forward) facing directions. P-values were combined across aerodynamic diameters of 0.542 – 10.366 µm for tests conducted with ARD, and 0.542 – 5.425 µm for sugar test aerosol. The overlay plots in figures 27 – 30 suggest that a horizontal orientation of all three inlets results in a negative sampling bias compared to the upright and upside down positions. The Tukey and Levene tests demonstrated no statistical differences between upright and upside down positions in the CATHIA and 3D printed inlets. Both resulted in a combined P-Value of 1.00 (greater than the alpha of 0.05), therefore failing to reject the null hypothesis. This concludes constant variance between upright and upside down

orientations for the CATHIA and 3D printed inlets. Figures 32 – 34 are example one-way analysis and Tukey test results in a single channel.

Additional comparison tests were conducted for the 3D printed inlet and SKC IMPACT sampler using sugar solution as the test aerosol and 0.253 m/s air velocity through the wind tunnel (Figure 31). ANOVA and Levene tests (Table 2) resulted in the combined P-Value of 1.00, concluding no statistical differences between the 3D printed inlet and SKC IMPACT sampler in 50 FPM wind speeds for particles up to 5 µm.

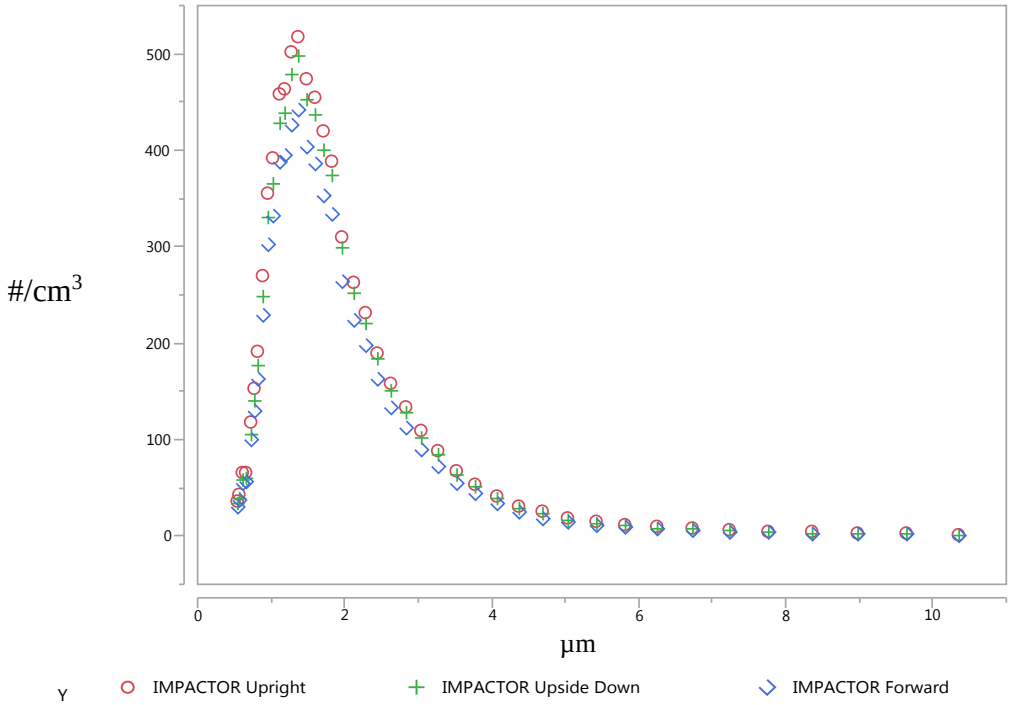


**Figure 27. SKC IMPACT Sampler Orientation Comparisons with ARD**

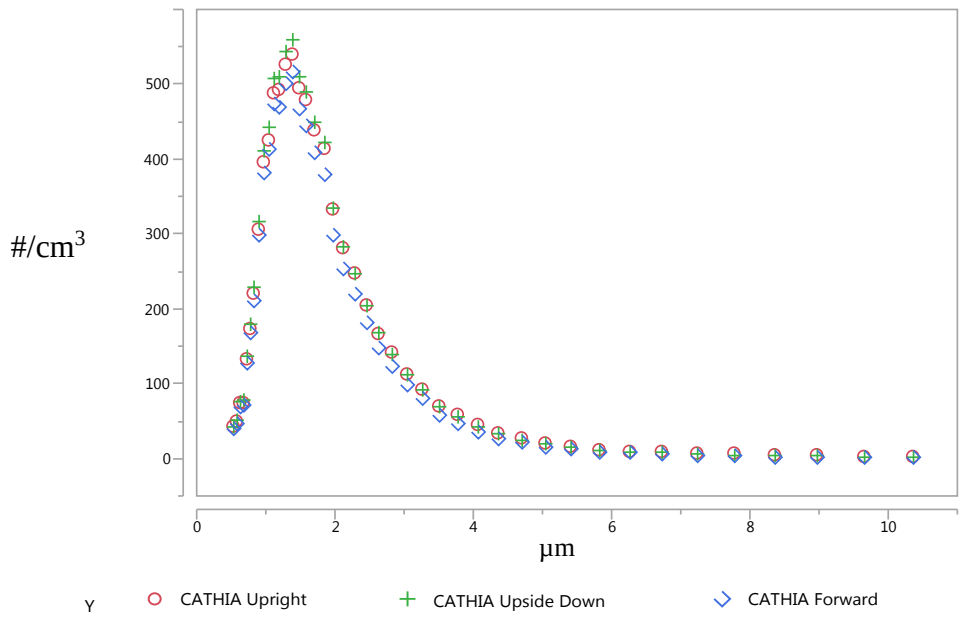


**Figure 28. CATHIA Orientation Comparisons with ARD**

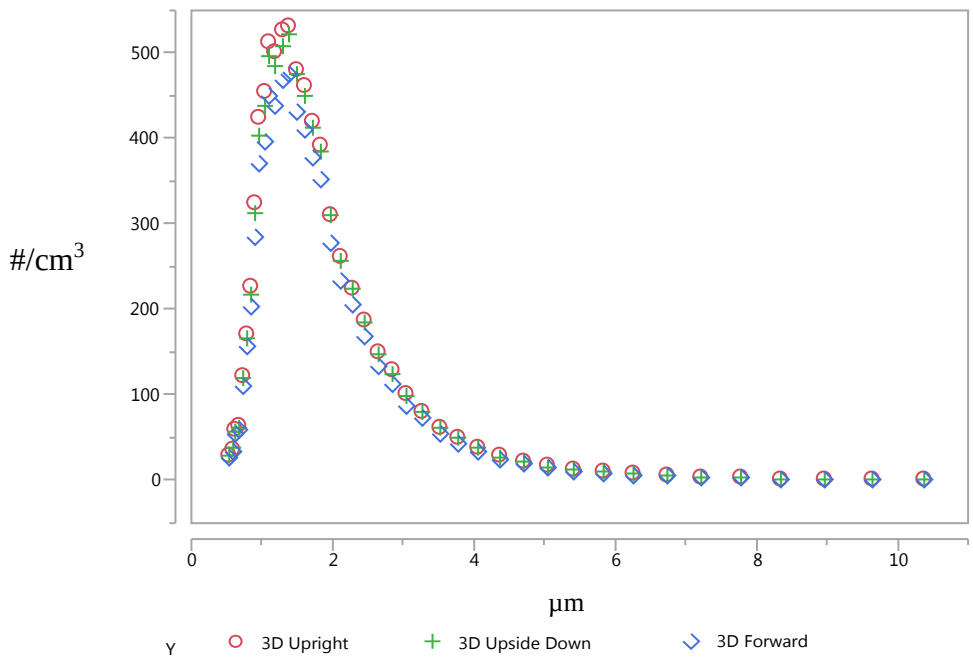


**Figure 29. 3D Printed Inlet Orientation Comparisons with ARD**

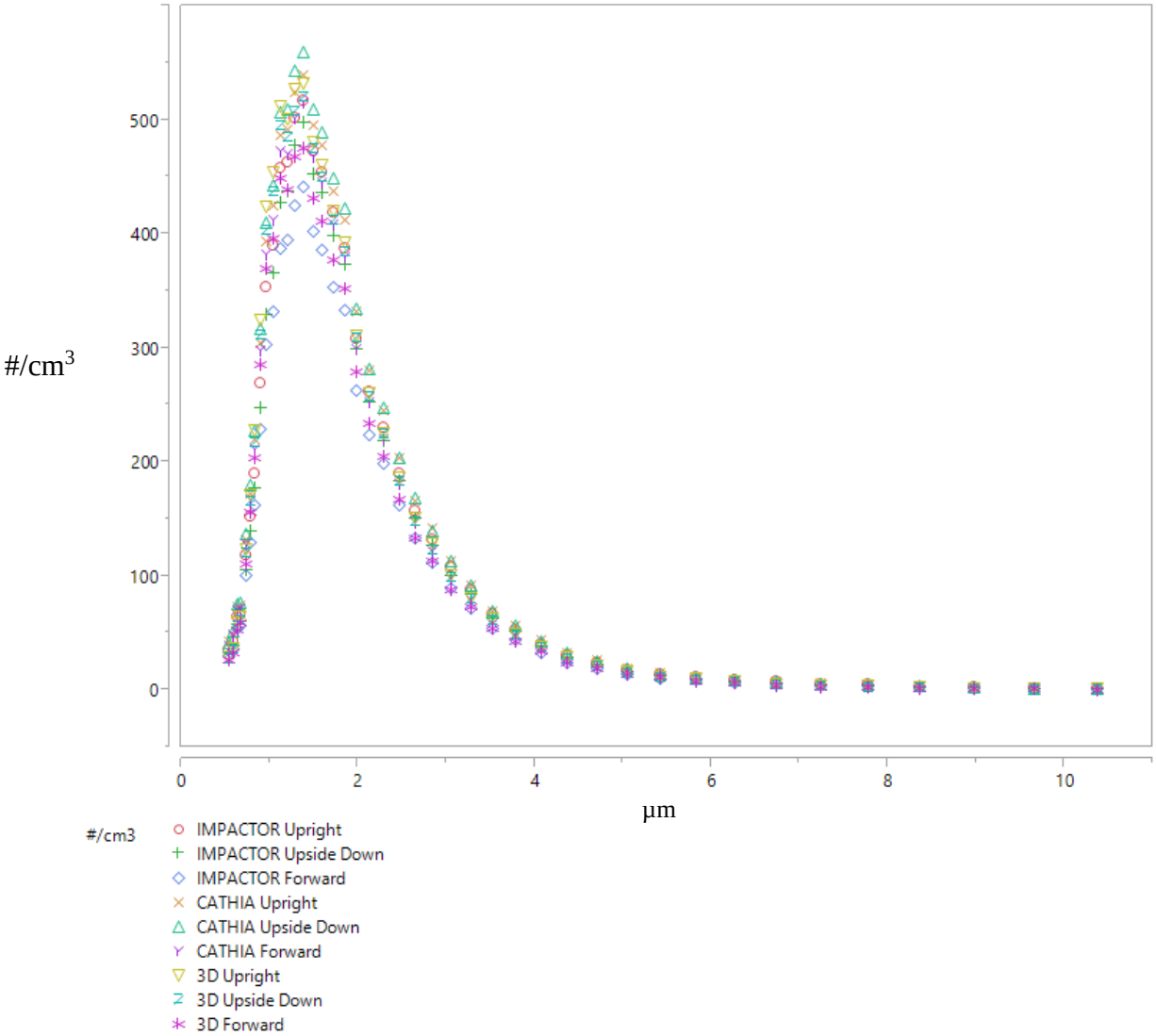


**Figure 30. Orientation Comparisons of SKC IMPACT SAMPLER, CATHIA, and 3D Printed Inlet with ARD**

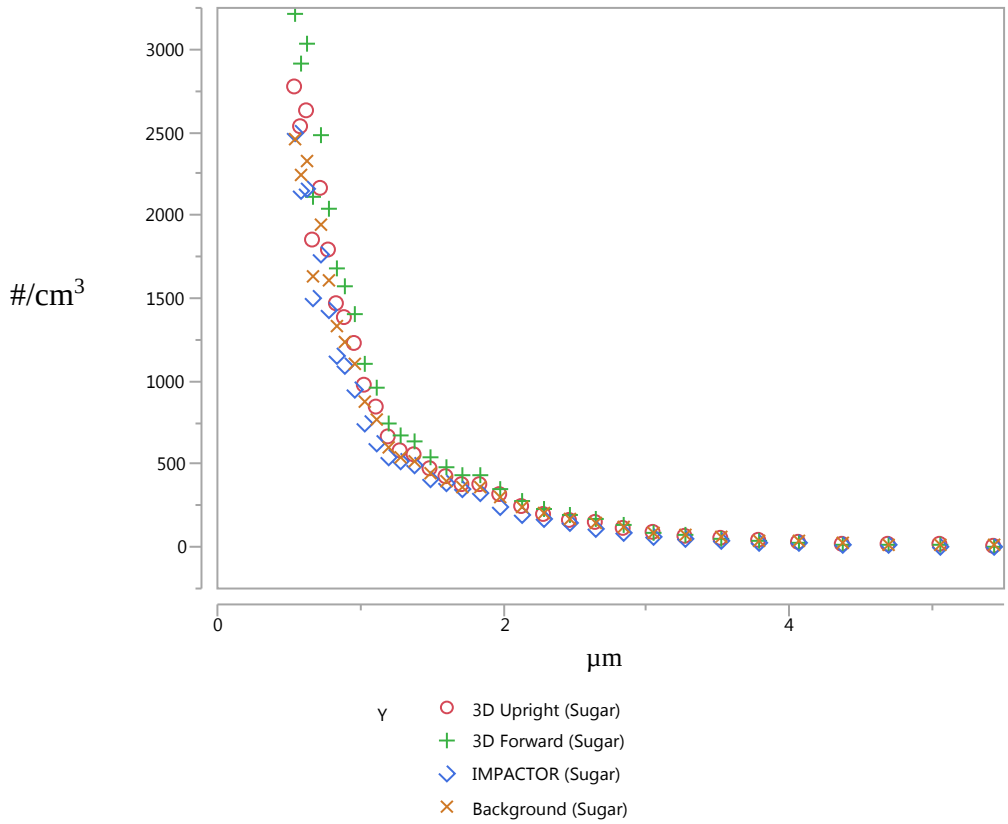


**Figure 31. Comparison of 3D Printed Inlet vs. SKC IMPACT SAMPLER in 0.254 m/s Wind Speed and Sugar Test Aerosol**

**Table 2. Combined P-Values of Aerosol Inlet Orientation Comparisons**

| Aerosol Sampling Inlet | Orientation Comparison | Test Aerosol | Statistical Test | P-value* |
|---|---|---|---|---|
| CATHIA | Upright/Upside Down/Forward | ARD | ANOVA | HS |
| CATHIA | Upright vs. Forward | ARD | ANOVA | HS |
| CATHIA | Upside Down vs. Forward | ARD | ANOVA | HS |
| CATHIA | Upright vs. Upside Down | ARD | ANOVA | NS |
| CATHIA | Upright/Upside Down/Forward | ARD | Levene | N/A |
| CATHIA | Upright/Upside Down/Forward | ARD | Welch's | HS |
| SKC IMPACT SAMPLER | Upright/Upside Down/Forward | ARD | ANOVA | HS |
| SKC IMPACT SAMPLER | Upright vs. Forward | ARD | ANOVA | HS |

*Statistically nonsignificant >0.05 (NS), Statistically significant <0.05 (S), Highly statistically significant <<0.05 (HS)

| Aerosol Sampling Inlet | Orientation Comparison | Test Aerosol | Statistical Test | P-value* |
|---|---|---|---|---|
| SKC IMPACT SAMPLER | Upside Down vs. Forward | ARD | ANOVA | HS |
| SKC IMPACT SAMPLER | Upright vs. Upside Down | ARD | ANOVA | HS |
| SKC IMPACT SAMPLER | Upright/Upside Down/Forward | ARD | Levene | N/A |
| SKC IMPACT SAMPLER | Upright/Upside Down/Forward | ARD | Welch's | HS |
| 3D Printed | Upright/Upside Down/Forward | ARD | ANOVA | HS |
| 3D Printed | Upright vs. Forward | ARD | ANOVA | HS |
| 3D Printed | Upside Down vs. Forward | ARD | ANOVA | HS |
| 3D Printed | Upright vs. Upside Down | ARD | ANOVA | NS |
| 3D Printed | Upright/Upside Down/Forward | ARD | Levene | N/A |
| 3D Printed | Upright/Upside Down/Forward | ARD | Welch's | HS |
| 3D Printed/SKC IMPACT SAMPLER | Upright (3D)/Forward (3D)/Upright (SKC IMPACT SAMPLER) | Sugar | ANOVA | NS |
| 3D Printed | Forward vs. Background | Sugar | ANOVA | NS |
| 3D Printed/SKC IMPACT SAMPLER | Forward (3D) vs. Upright (SKC IMPACT SAMPLER) | Sugar | ANOVA | NS |
| 3D Printed | Forward vs. Upright | Sugar | ANOVA | NS |
| 3D Printed | Upright vs. Background | Sugar | ANOVA | NS |
| 3D Printed/SKC IMPACT SAMPLER | Upright | Sugar | ANOVA | NS |
| 3D Printed/SKC IMPACT SAMPLER | Upright (3D)/Forward (3D)/Upright (SKC IMPACT SAMPLER) | Sugar | Levene | NS |
| 3D Printed/SKC IMPACT SAMPLER | Upright (3D)/Forward (3D)/Upright (SKC IMPACT SAMPLER) | Sugar | Welch's | NS |

*Statistically nonsignificant >0.05 (NS), Statistically significant <0.05 (S), Highly statistically significant <<0.05 (HS)

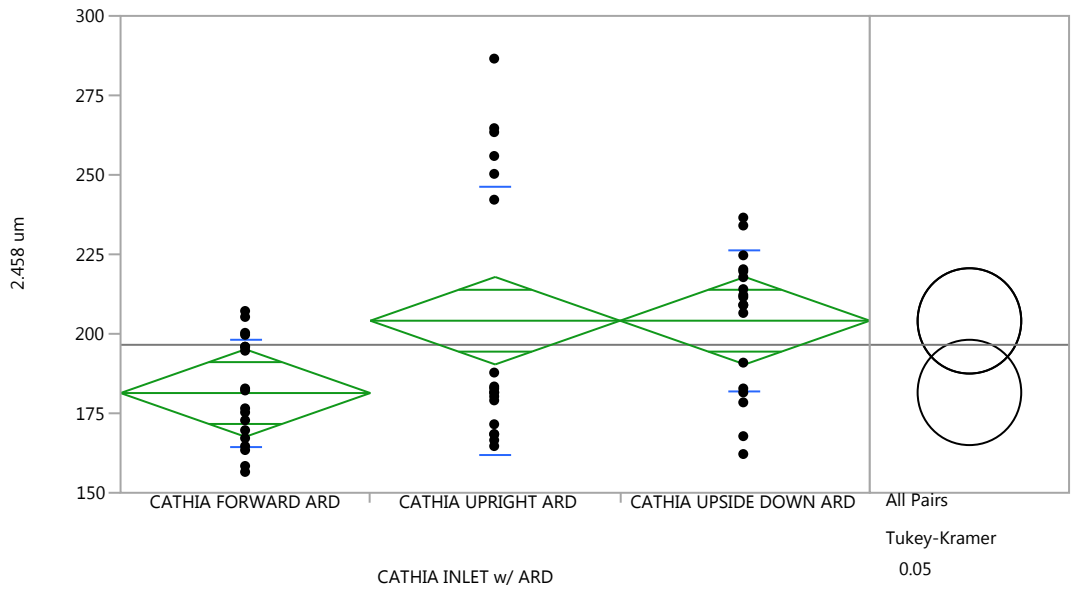


**Figure 32. One-way Analysis of 2.458 µm by CATHIA Inlet Orientations with ARD**

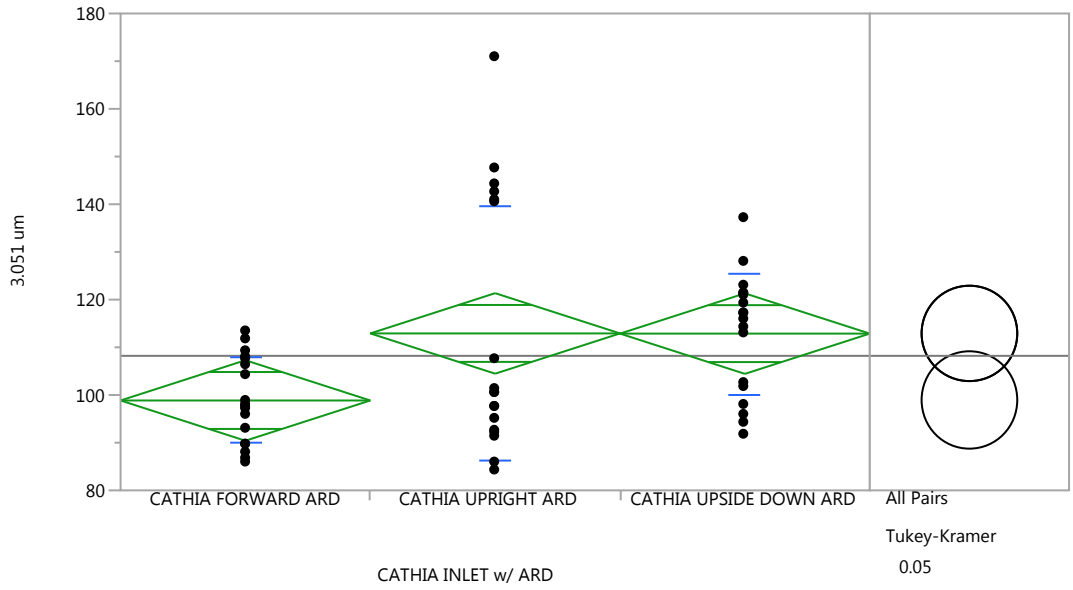


**Figure 33. One-way Analysis of 3.051 µm by CATHIA Inlet Orientations with ARD**

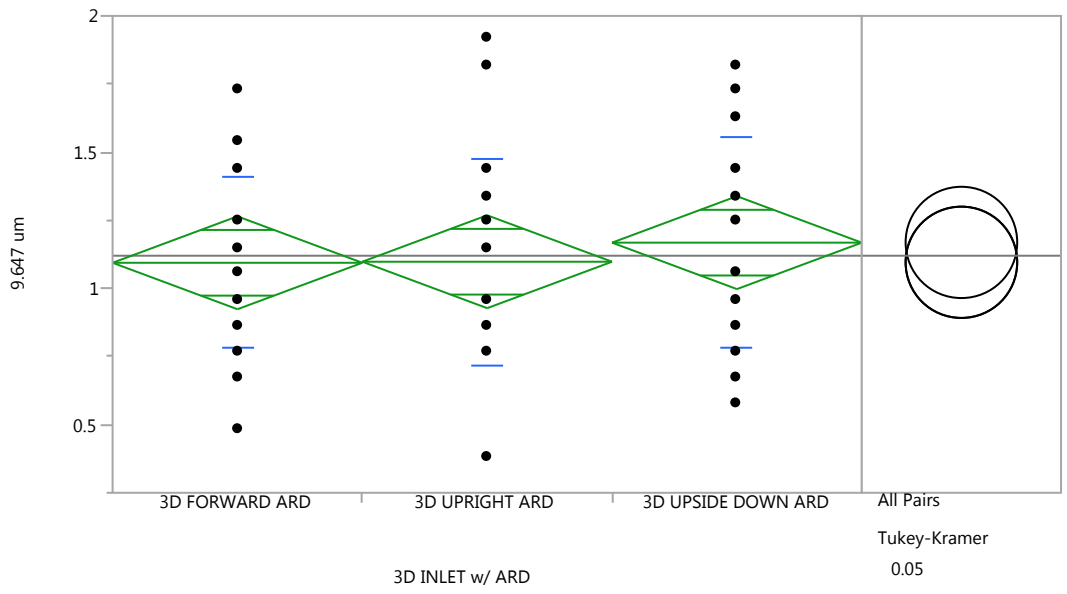


**Figure 34. One-way Analysis of 9.647 µm by 3D Printed Inlet Orientations with ARD**

**Aerosol Inlet Mounted on UAS (On vs. Off)**

Aerosol inlets were mounted on the UAS and sampling comparisons were conducted when the UAS was on versus off. At a wind speed of 0 m/s and ARD as the test aerosol, the SKC IMPACT sampler resulted in a negative sampling bias at an average of -18.8% when the UAS was on compared to off (Figure 35). The 3D printed inlet and CATHIA had a positive particle count concentration sampling bias, 12.5% and 7.6% respectively (Figure 36, Figure 37) by particle count concentration for particle size ranging from 0.542 – 10.366 µm. The average particle count percent difference for UAS on and off comparisons for the candidate inlets with a 95% confidence interval are presented in Figure 39. Five bins were grouped for the APS size channels 0.542 – 8.977

µm. Figure 40 displays a smoothed line graph of the average particle count percent difference for UAS on and off comparisons; to even out fluctuations in the data, a moving average trendline with a period set to 15 was selected. Both when the UAS was on and off, the SKC IMPACT sampler collected 1.5% more particles by count concentration than the CATHIA and 3.5% more than the 3D printed inlet. The ANOVA and Levene tests demonstrated no statistical differences for the SKC IMPACT sampler when the UAS was on compared to off. The ANOVA resulted in a P-Value of 0.9958 while the Levene test resulted in a P-value of 0.9793 (failing to reject the null hypothesis) (Table 3). Figure 38 presents sampling comparisons with all three candidate inlets.

The WVU wind tunnel was set at a wind speed of 0.254 m/s to determine the sampling bias of the three inlets while simulating hovering and forward flight for the UAS for particles sizes generated at 0.542 – 5.425 µm. Comparison tests conducted in the wind tunnel resulted in a negative sampling bias for all inlets (Figure 44). The SKC IMPACT sampler had the least sampling bias among the three (-52.7%) (Figure 41), while the 3D printed inlet resulted in the largest percent difference at -70.6% (Figure 42) and the CATHIA resulted in a -56.6% difference (Figure 43). Five bins were grouped for the APS size channels 0.542 – 5.425 µm and the average particle count percent difference for UAS on and off comparisons for the candidate inlets with a 95% confidence interval are presented in Figure 45. Figure 46 displays a smoothed line graph of the average particle count percent difference for UAS on and off comparisons at a cross-sectional wind velocity of 0.254 m/s; a moving average trendline with a period set to 8 was selected.

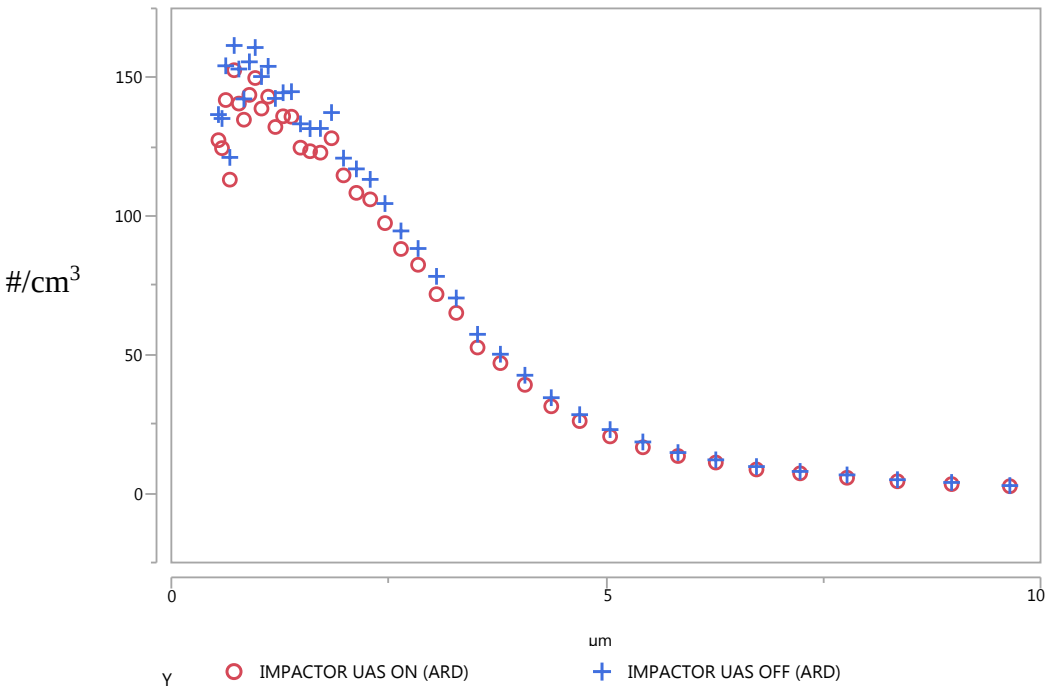


**Figure 35. UAS On vs Off Comparison for SKC IMPACT Sampler with ARD**

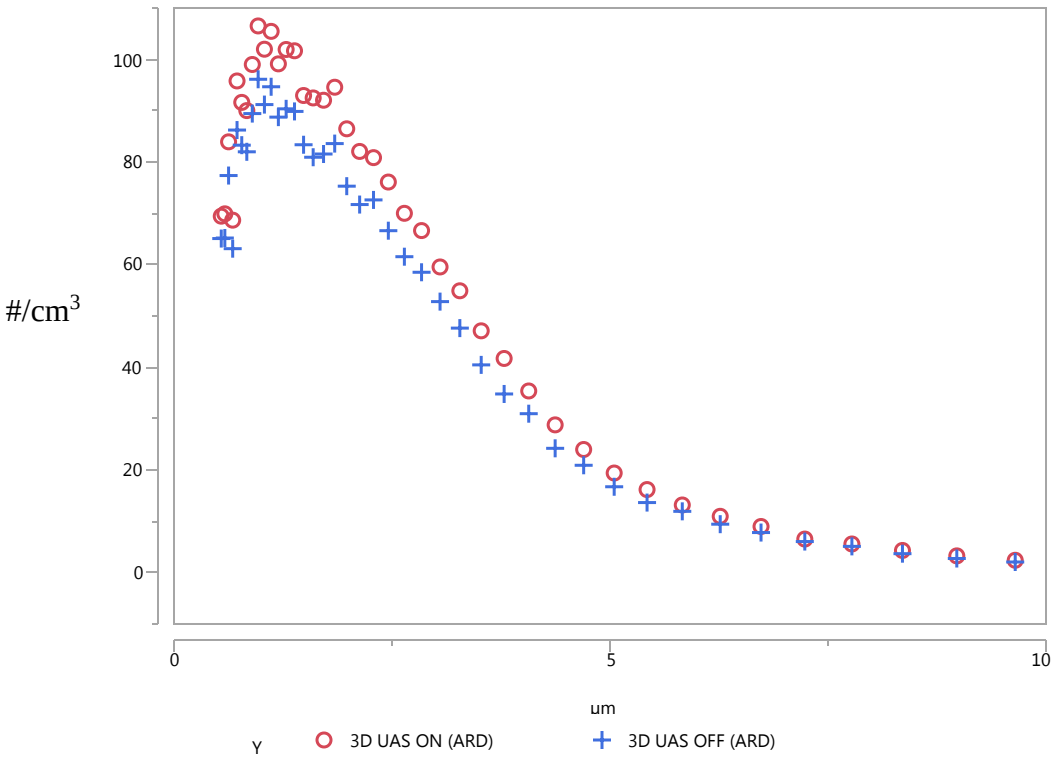


**Figure 36. UAS On vs Off Comparison for 3D Printed Inlet with ARD**

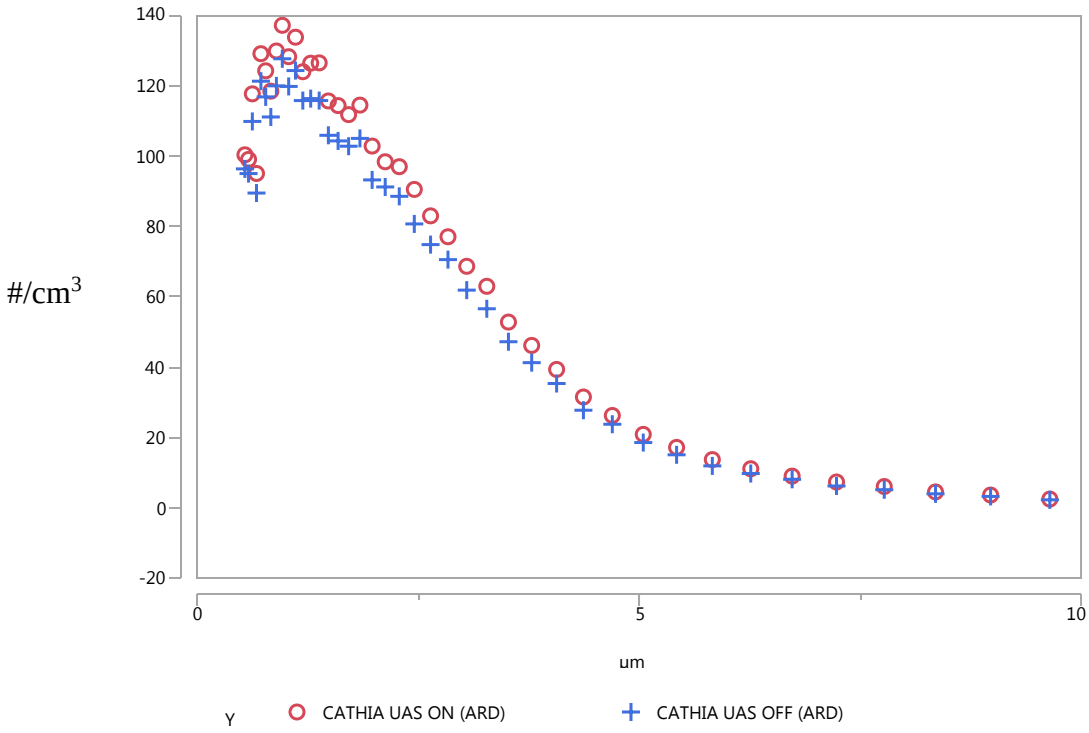


**Figure 37. UAS On vs Off Comparison for CATHIA with ARD**

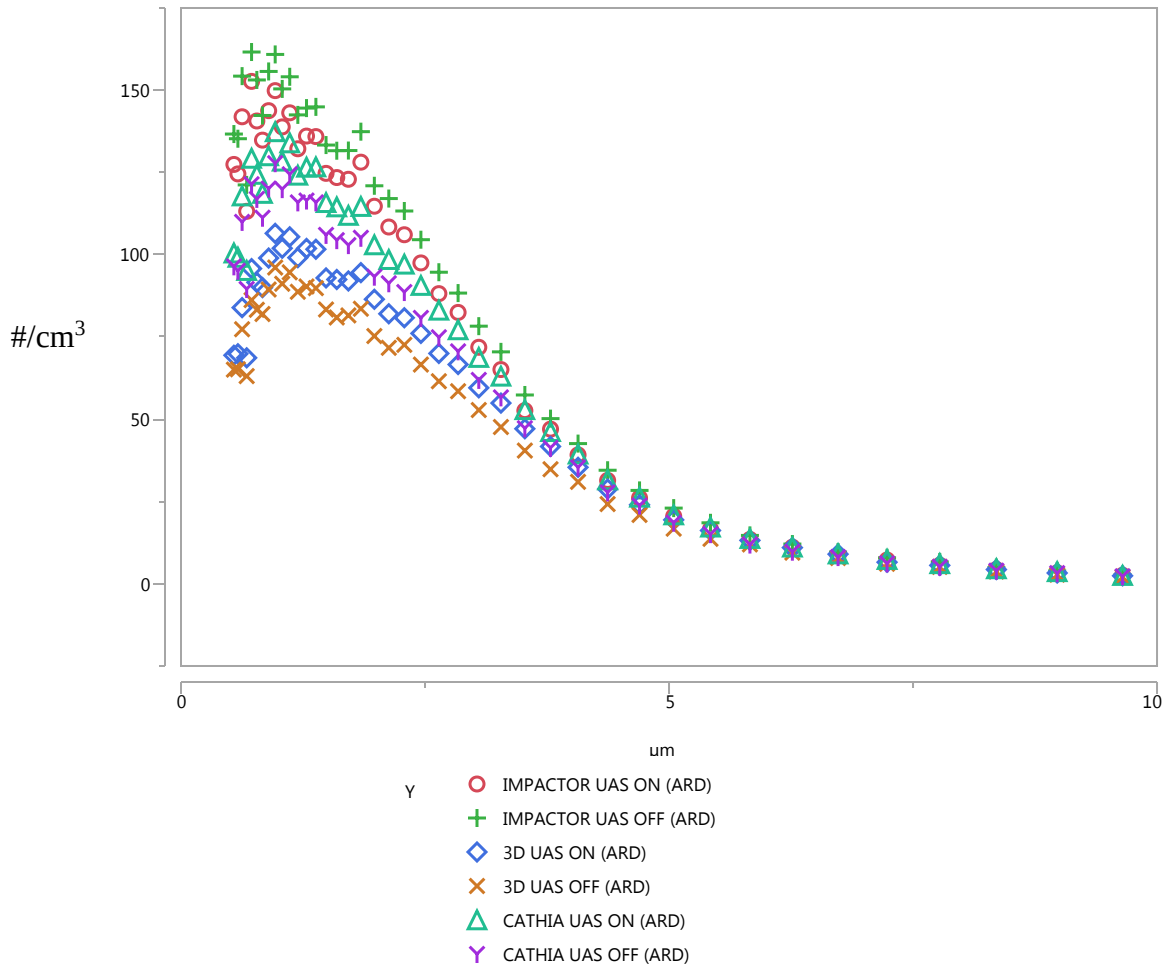


**Figure 38. UAS On vs Off Comparison for SKC IMPACT Sampler, 3D Printed Inlet, and CATHIA with ARD**

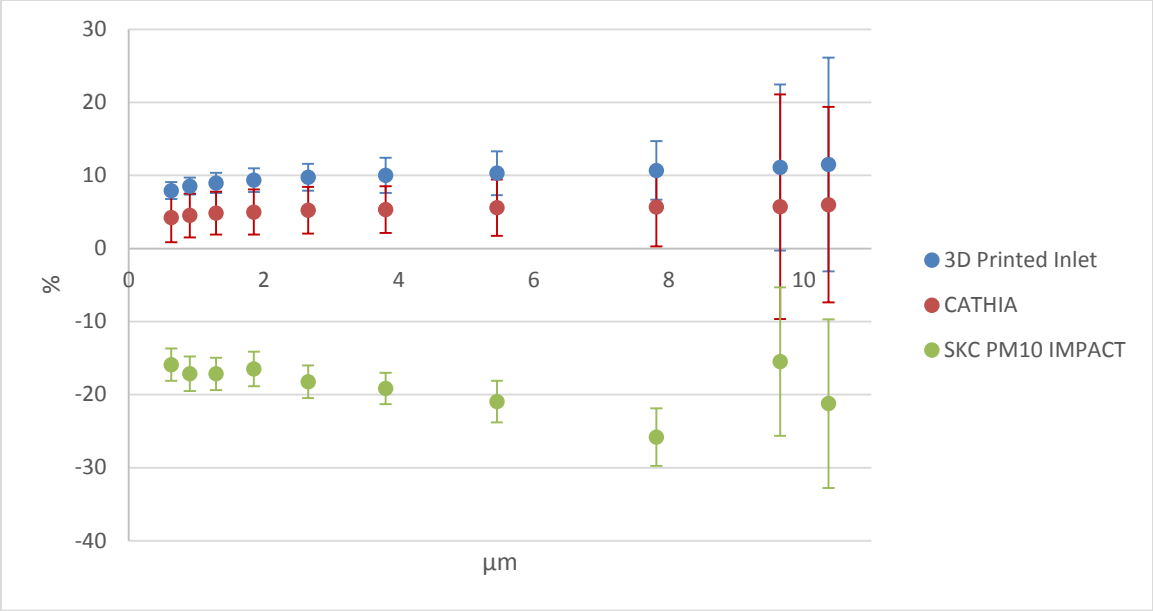


**Figure 39. Particle Count Percent Difference UAS On vs Off Comparison for Inlets with ARD in UC Aerosol Chamber with 95% Confidence Interval (combined size bins)**

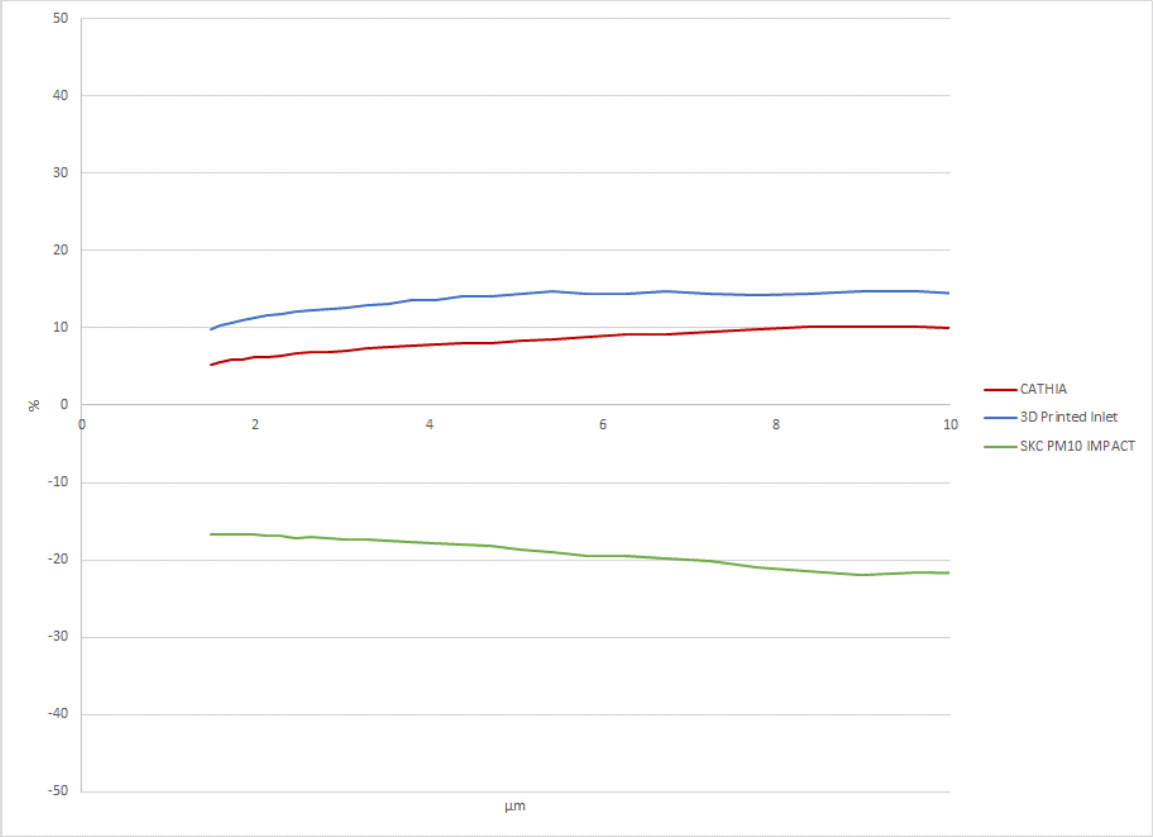


**Figure 40. Measure of Central Tendency of Particle Count Percent Difference UAS On vs Off Comparison for Inlets with ARD in UC Aerosol Chamber (smooth lines)**

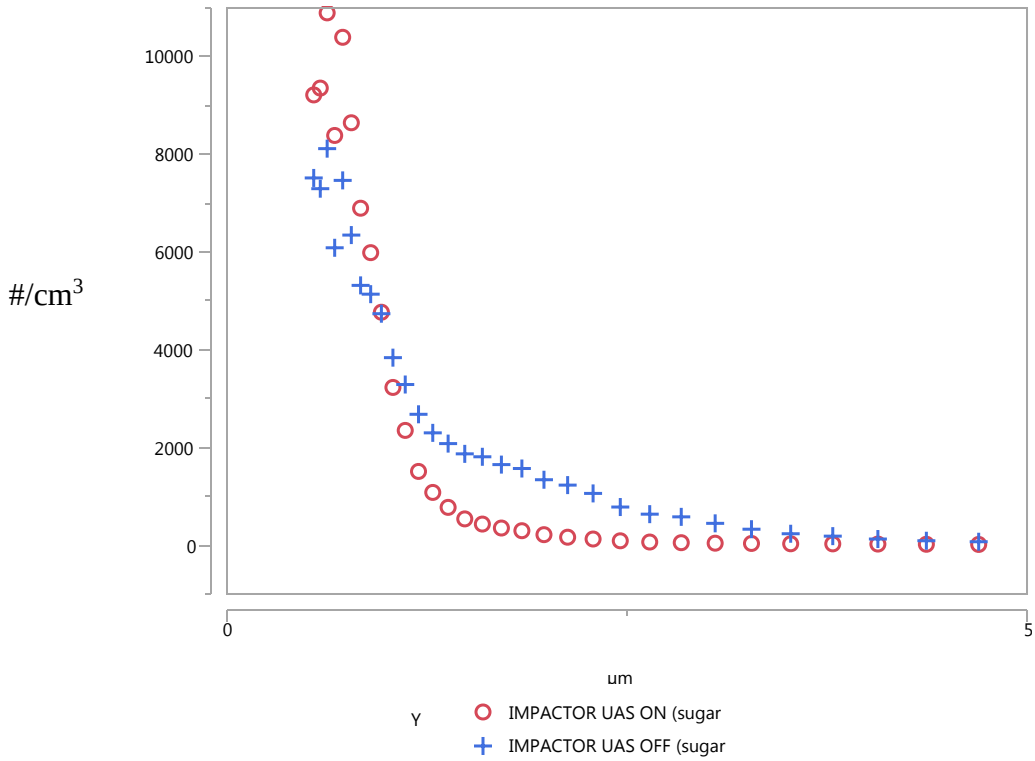


**Figure 41. UAS On vs Off Comparison for SKC IMPACT Sampler with Sugar and 0.254 m/s Wind Tunnel Speed**

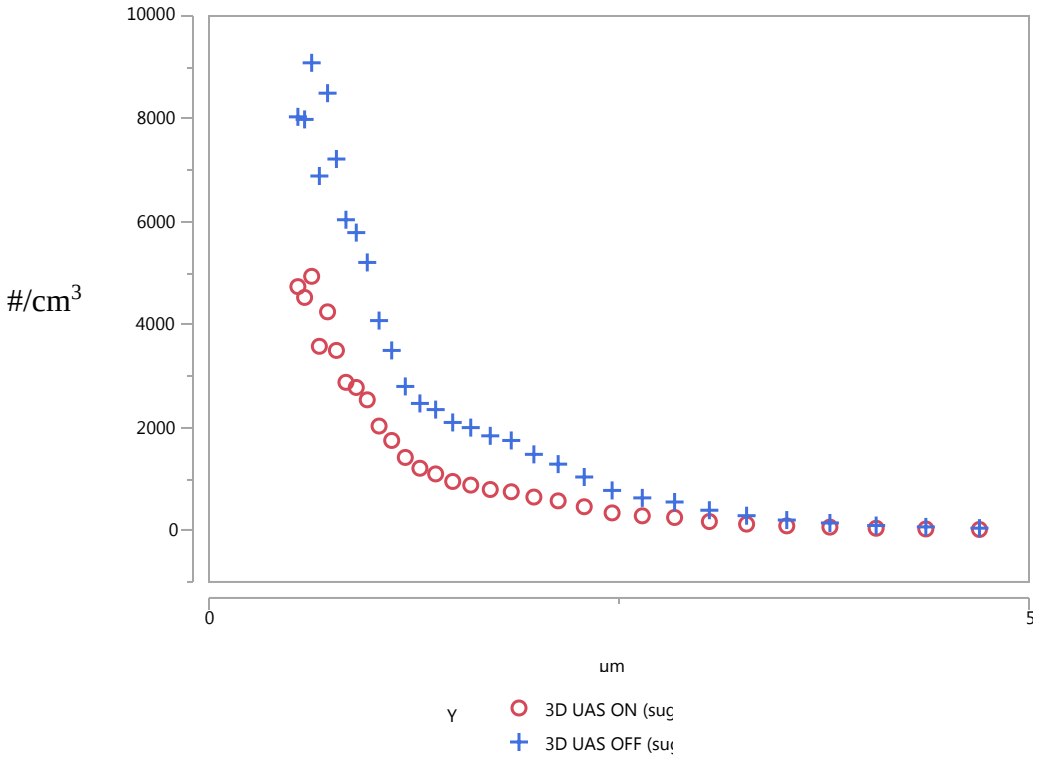


**Figure 42. UAS On vs Off Comparison for 3D Printed Inlet with Sugar and 0.254 m/s Wind Tunnel Speed**

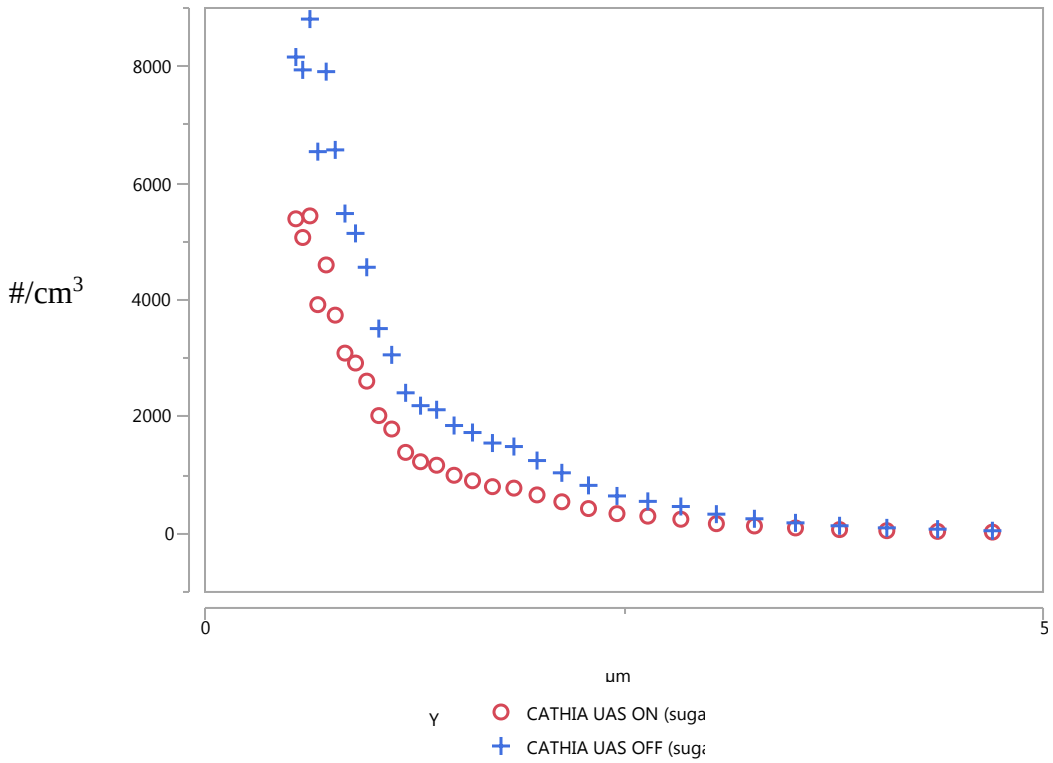


**Figure 43. UAS On vs Off Comparison for CATHIA with Sugar and 0.254 m/s Wind Tunnel Speed**

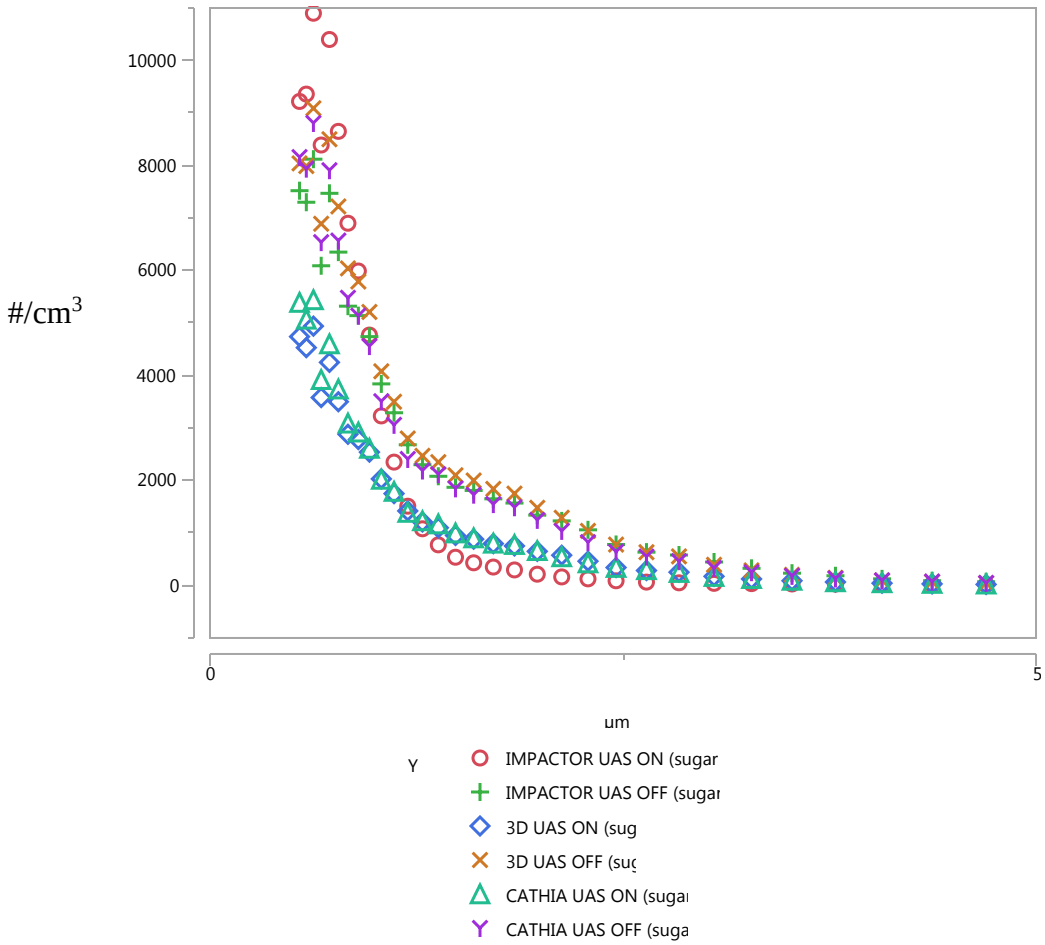


**Figure 44. Particle Count Concentration UAS On vs Off Comparison for SKC IMPACT Sampler, 3D Printed Inlet, and CATHIA with Sugar and 0.254 m/s Wind Tunnel Speed**

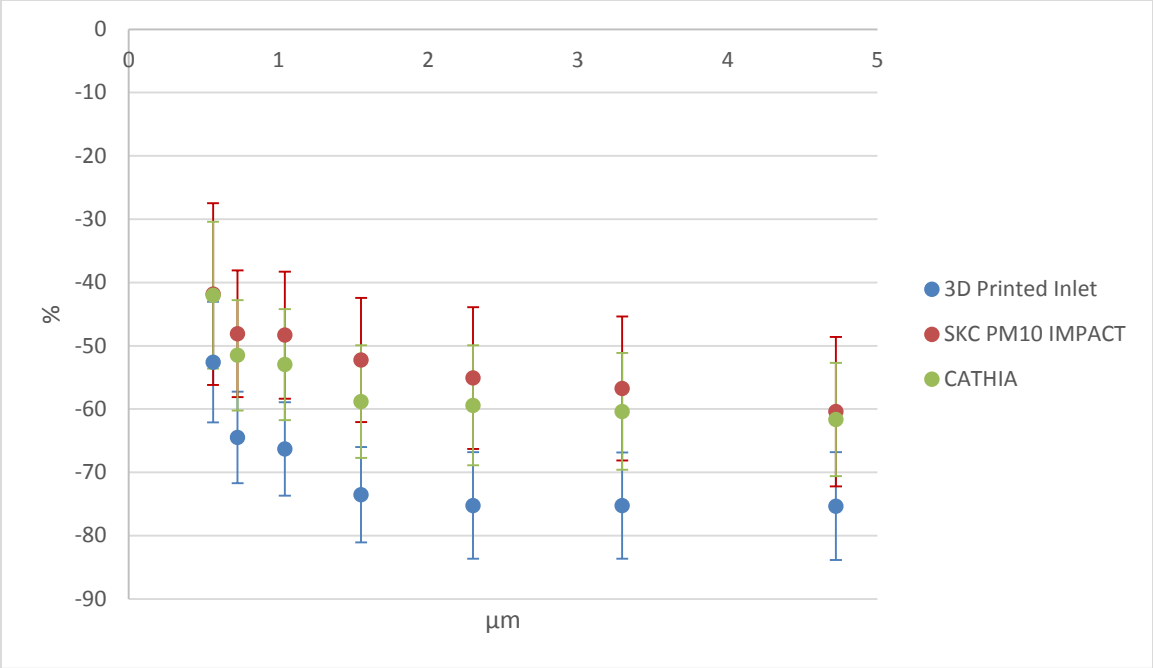


**Figure 45. Percent Difference UAS On vs Off Comparison for SKC IMPACT SAMPLER, 3D Printed Inlet, CATHIA with Sugar and 50 FPM Wind Tunnel Speed with 95% Confidence Interval (combined bins)**

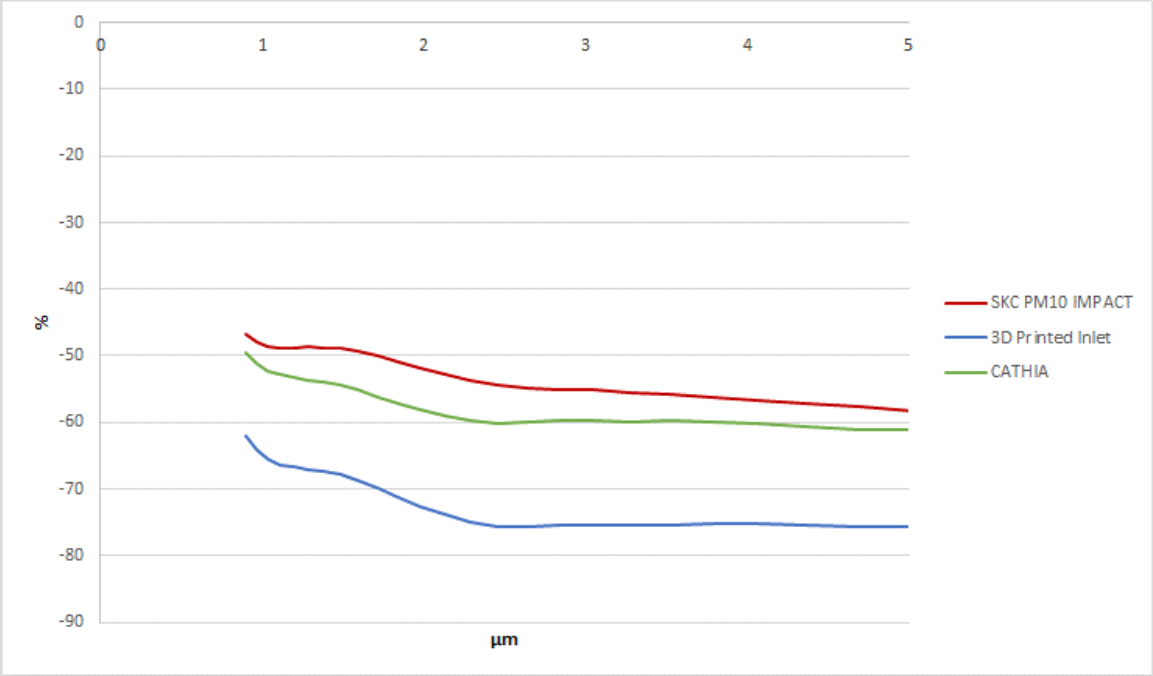


**Figure 46. Measure of Central Tendency of Percent Difference UAS On vs Off Comparison for SKC IMPACT SAMPLER, 3D Printed Inlet, CATHIA with Sugar and 0.254 m/s Wind Tunnel Speed (smooth lines)**

**Table 3. Combined P-Values of UAS "On" vs. "Off" Comparisons**

| Aerosol Sampling Inlet | Test Aerosol | Statistical Test | P-value |
|---|---|---|---|
| SKC IMPACT SAMPLER | ARD | ANOVA | NS |
| SKC IMPACT SAMPLER | ARD | Levene | NS |
| SKC IMPACT SAMPLER | Sugar | ANOVA | HS |
| SKC IMPACT SAMPLER | Sugar | Levene | HS |
| 3D Printed | ARD | ANOVA | HS |
| 3D Printed | ARD | Levene | S |
| 3D Printed | Sugar | ANOVA | HS |
| 3D Printed | Sugar | Levene | HS |
| CATHIA | ARD | ANOVA | HS |
| CATHIA | ARD | Levene | HS |
| CATHIA | Sugar | ANOVA | HS |
| CATHIA | Sugar | Levene | NS |

*Statistically nonsignificant >0.05 (NS), Statistically significant <0.05 (S), Highly statistically significant <<0.05 (HS)

# V. Discussion

The objective of this research was to contribute to the understanding of aerosol sampling and collection bias using a contemporary multi-rotor UAS as a sampling platform. Optimal configurations for aerosol particle collection on a multi-rotor, small UAS were determined. The results of this research observed significant influences on sampling efficiency from the UAS and a cross-sectional wind velocity.

## Specific Aim 1 Revisited

The first specific aim was UAS airframe airflow characterization. Results from experiment 1 are consistent with the findings in the study conducted by Hwang et al. (2015). A strong downwash flow was observed from the airflow visualization results. In order not to disrupt the center of gravity of the UAS, the two main locations of consideration for aerosol inlet mounting were directly above or below the fuselage. The airflow velocity measured above the fuselage resulted in a flow rate more than two times greater than below the fuselage. Directly below the fuselage of the UAS was the optimal placement for an air sampling inlet to achieve minimal sampling bias. However, the mounting plate and placement of the UAS battery limited the possible orientations of the inlets. The small size of the SKC PM10 IMPACT sampler allowed its mounting location to be placed in the center of the plate in the upright position. The 3D printed inlet was also positioned upright, but had to be placed at the end of the mounting plate because of its size and location of the battery. Although the placement of CATHIA was ideal, its orientation was not. The weight and long length of the CATHIA sampler forced a horizontal orientation for UAS mounting.

**Specific Aim 2 Revisited**

Specific aim 2 was the assessment of existing and modified aerosol collections designs to minimize bias. Although no modifications were made on the existing CATHIA and IMPACT samplers, modifications were made to a patent design (Raabe and Teague, 1995) and produced in a 3D printer. In experiment 2, sampling efficiencies at three orientations for the selected inlets were assessed. A horizontal orientation of all three inlets resulted in a negative sampling bias compared to the upright and upside down positions. The results from experiment 2 are consistent with the study conducted by Jones et al. (2005) on the performance of thoracic size-selective sampling where the CATHIA slightly oversampled another impactor based pre-selector. When compared to the IMPACT sampler, the 3D printed inlet has a negative sampling bias but does follow the theory of impactors being capable of providing the size distribution of an aerosol between 0.5 – 10 µm. The three selected inlets were not compared to a reference sampler and their adherence to the thoracic convention could not be determined. The Tukey and Levene tests demonstrated no statistical differences between upright and upside down positions in the CATHIA and 3D printed inlets. There were significant statistical differences between upright and upside down orientations for the IMPACT sampler; rearrangements for its mounting would not be recommended for minimal sampling bias.

**Specific Aim 3 Revisited**

Specific aim 3 was sampling bias determination for UAS airframe and aerosol sampling in simulated hovering and forward flight. Particle size sampling bias characterization was met with experiments 2 and 3. Experiment 2 was set to represent a

still-air environment while experiment 3 represented a low to calm air environment. The cross-sectional velocity in the wind tunnel was set to 0.254 m/s; the UAS is capable of traveling and maintaining a hover at low wind speeds. Limitations in representing both hovering and forward flight include the lack of measurement of the UAS tilt angle and insufficient varying increased cross-sectional airflow.

Limitations in aerosol generation may have contributed to bias in sampling efficiency results of comparisons with and without UAS rotor employment. Particularly in experiment 2, the aerosol generator has not been quantified for use with ARD as a test aerosol. Without ventilation in the UC aerosol chamber, wall effects and resuspension of ARD may have contributed some bias. Although the GRIMM was used to measure uniformity, aerosol concentrations between each collected sample were not exact. Additionally, there were inconsistencies in the sampling results between tests conducted in the UC chamber and the WVU wind tunnel. In experiment 2 the IMPACT sampler had the greatest percent difference in sampling efficiencies comparing UAS on and off scenarios; on the other hand, experiments conducted in the wind tunnel results with the IMPACT sampler possessing the least bias. Some inconsistency of aerosol concentrations between sample collections may have contributed to greater variability. The CPC was used to record uniformity of test aerosol concentrations in the wind tunnel. An average of 44% more particles by count concentration were present when the UAS was turned off for the IMPACT sampler compared to concentrations in the wind tunnel for the CATHIA and 3D printed inlet. This may suggest that overtime, the concentration of the sugar solution increased in the six-jet atomizer as the solution slowly diluted.

However, there were no significant differences in average particle count concentrations between sampling collections for each aerosol sampling inlet.

The mounting positions and locations of the selected inlets may have also contributed to the variability in results. The SKC IMPACT sampler was placed directly center of the mounting plate, while the 3D printed inlet and CATHIA inlet nozzles were situated at the edge of the mounting plate. Because each of the three inlets were not placed in the same location, differences in the sample volume of air and effect of turbulence at their respective locations under the fuselage could have contributions to bias.

Tests conducted in experiment 3 show influences on sampling efficiency from the UAS and a cross-sectional wind velocity. All three selected inlets resulted in a negative sampling bias from these influences. This effect and bias direction are consistent with sampler inlet efficiency recommendations from Baron (2016) where PM10 and thoracic samplers are expected to be susceptible to wind effects. In figure 46, the graphical results displays a significant decrease in sampling efficiency for all three inlets near the 1 µm aerodynamic diameter. This observation suggests the downwash turbulence of the UAS and mounting location of the inlets may have contributed to this result. Overall, the CATHIA demonstrated the least sampling bias susceptibility introduced from the UAS rotors and cross-sectional wind speed even at a horizontal orientation.

**Summary**

A summary of the results and observations include:

- A significant downwash flow was induced by the rotors and propellers.

- Below the fuselage of the UAS was the optimal placement for an air sampling inlet.
- A horizontal orientation of all three inlets resulted in a negative sampling bias and significant statistical difference compared to the upright and upside down orientations.
- No significant statistical difference for sampling efficiency for the upright and upside down orientations for CATHIA and 3D Printed inlets.
- SKC IMPACT sampler resulted in a negative sampling efficiency bias at -18.8% comparing rotor employment in the still air chamber.
- CATHIA and 3D printed inlet resulted in a positive sampling efficiency bias at 7.6% and 12.5%, respectively comparing rotor employment in the still air chamber.
- For all three aerosol samplers, a combination of turbulence from UAS rotors and cross-sectional airflow significantly reduced sampling efficiencies compared to when UAS rotors were off.

# VI. 3D Printed Universal Inlet

## Introduction

In the patent for a Universal Inlet for Airborne-Particle Size-Selective Sampling invented by Raabe and Teague (1995), parallel jet orifices, collector holes, and stagnation chambers operate together as a size-selective airborne particle sampling device. This candidate inlet was selected primarily due to its operational independence to wind direction and speed. The use of in-house 3D printed air sampling inlets has not been widely explored or well characterized in the literature. Lee et al (2016) developed a respirable size-selective sampler for end-of-shift quartz measurement constructed with a Fortus 360mc 3D printer loaded with ABS-M30 material. In their study, Lee et al. concluded that the 3D printed cyclone resulted in minimum bias when compared to the ACGIH respirable convention. This chapter will summarize the utility of 3D printed inlets as an effective size-selective sampler.

## Design Process

The universal size selective inlet is designed for larger particles to be separated by inertial collection as they are drawn into the sampler. The incoming air stream exits jet orifices aligned with the collector holes and leads to a closed stagnation chamber, where the larger particles (>10 µm) are entrapped. Smaller particles 10 µm and below are carried by the airstream that passes the collector holes into the small particle collection connector.

The desired cut size for the aerosol sampling inlet can be calculated by Stokes scaling. Adjustments can be made to the diameter of the flow holes, number of flow hole collectors, or sampling flow rate using the following equation:

$$ECD_{ar} = \sqrt{\frac{9\eta WSt}{u\rho}} \tag{5}$$

Where, $ECD_{ar}$ is the effective cutoff aerodynamic diameter, η is the dynamic viscosity of air, W is the flow hole orifice diameter, *St* is Stokes' number, *u* is the flow velocity, and ρ is the particle density. The Raabe and Teague (1995) design is characterized for a Stokes' number of 0.2. The particular design that was printed has a desired aerodynamic cut size of 10 µm. To achieve a cut size of 10 µm and an operational sampling flow rate of 10 LPM, 8 flow holes with a diameter of 0.43 cm and depth of 0.43 cm were determined from equation 5. Adjacent to the flow holes were 8 collector holes leading to the stagnation chamber with a diameter of 0.46 cm and a depth of 0.15 cm. The distance between the flow holes to the collector holes were set to 0.43 cm.

**Design Modifications**

The original eight component patent design was modified to six main component parts. Because the intended use of the 3D printed inlet was aerosol sampling capability on a small unmanned aerial system, the mesh screen plate to keep insects from entering the inlet was eliminated from the original design. The sharp-edged fan-plate was modified to increase durability of the 3D print (Figure 52). The patent designed the bell-cap and collector holes as two separate pieces to be held together by two screws. In the modified 3D print, the bell-cap and collector holes were designed as a single unit with

lock-and-key attachments from the collector holes to bottom base and fan plate (Figure 51, Figure 53). This modification ensured an air-tight seal from the top and bottom of the collector holes, compared to the original two screw pin design. A conical attachment was also added to the design to allow a 0.952 cm tubing connection to a high flow pump.

The six main components of the universal inlet patent design (bell cap with flow holes, stagnation chamber collector holes, fan plate, base plate, suction tube section, conical air pump connector) were developed using Dassault Systèmes SolidWorks Corporation software (2013-2014 edition) and produced with a 3D Systems, Inc. ProJet 3500 Max three-dimensional printer (Figure 47, Figure 48). The part material loaded in the printer is VisiJet M3 Black, which is a high strength and flexibility plastic. Properties of the plastic material include a liquid density of 1.02 g/cm$^3$ at 80 C, tensile strength of 35.2 MPa, and a flexural strength of 44.5 MPa (3D Systems, 2015). Once printed, the bottom of the collector hole plate was coated with Dap and Peel temporary caulk to reduce particle rebound or re-entrainment. Dap and Peel was used as a seal between all components to minimize leakage.

**Figure 47. Exploded View of Six Component 3D Printed Inlet**

**Figure 48. Assembled 3D Printed Inlet**

## Inlet Characterization

The 3D printed inlet was characterized in an aerosol chamber at the University of Cincinnati, and compared with the well-characterized SKC IMPACT PM10 sampler. Tests were conducted with Arizona Road Dust 5 (ARD 5) which has a nominal aerodynamic diameter ranging between 0.5 to 10 µm. The test aerosol was generated with an air pump producing 12.5 LPM of air into three 6-jet Collison Nebulizers (BGI Inc., Waltham, MA, USA) containing the ARD 5. A small horizontal fan suspended the aerosol, while an offset vertical fan dispersed the aerosol in the direction of the inlet. The

concentration of aerosols in the chamber was determined by a GRIMM portable aerosol counter, and was constantly measured to ensure uniformity between sample collections.

The exiting nozzle of the PM10 IMPACT sampler and 3D printed inlet were connected to an aerodynamic particle sizer (APS). A flow divider directed flow toward both the APS analyzer and to a A.P Buck Libra Plus LP-20 high flow pump. Flow rates through each air sampling inlet were determined by pre and post calibration using a TSI 4000 Series Model 4045 G mass flowmeter. The IMPACT sampler was calibrated with the SKC calibration adapter, while the 3D printed inlet was calibrated with a modified air tight calibration jar (Figure 49, 50). Two minute samples were taken in sequence, alternating the IMPACT and 3D printed inlets.

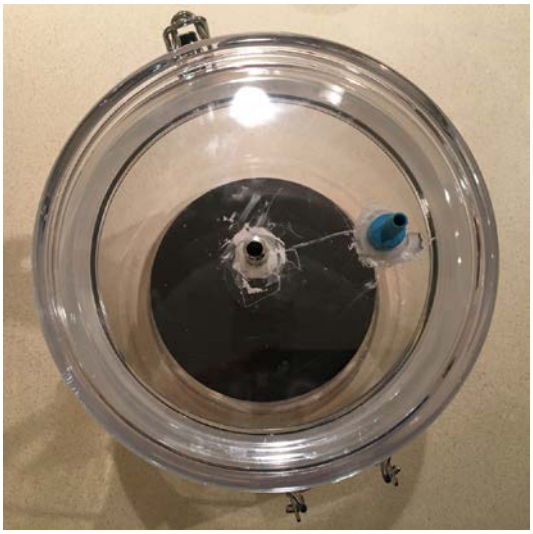

**Figure 49. Top View of Calibration Jar**

**Figure 50. 3D Printed Inlet Calibration Jar**

**Figure 51. Side-by-side comparison of initial design (left) and revised design (right) of Base Plate**

**Figure 52. Side-by-side comparison of initial design (left) and revised design (right) of Fan Plate**

**Figure 53. Side-by-side comparison of initial design (left) and revised design (right) of Bell Cap**

**Results**

Tests were conducted to compare the 3D printed inlet with the well characterized SKC IMPACT SAMPLER. The comparative results show a -7.2% difference for particle sizes between 0.5 – 10 µm (Figure 55). The largest difference occurs are between the 7.2 – 10.4 µm particle size range at 51.3% difference. The ANOVA and Levene tests demonstrated the least statistical difference at the aerodynamic particle size of 2.129 µm (Figure 54). Both resulted in a combined P-Value of 0.9542 greater than the alpha of 0.05, therefore failing to reject the null hypothesis. This concludes constant variance between the SKC IMPACT SAMPLER and 3D Printed inlet at 2.129 µm.

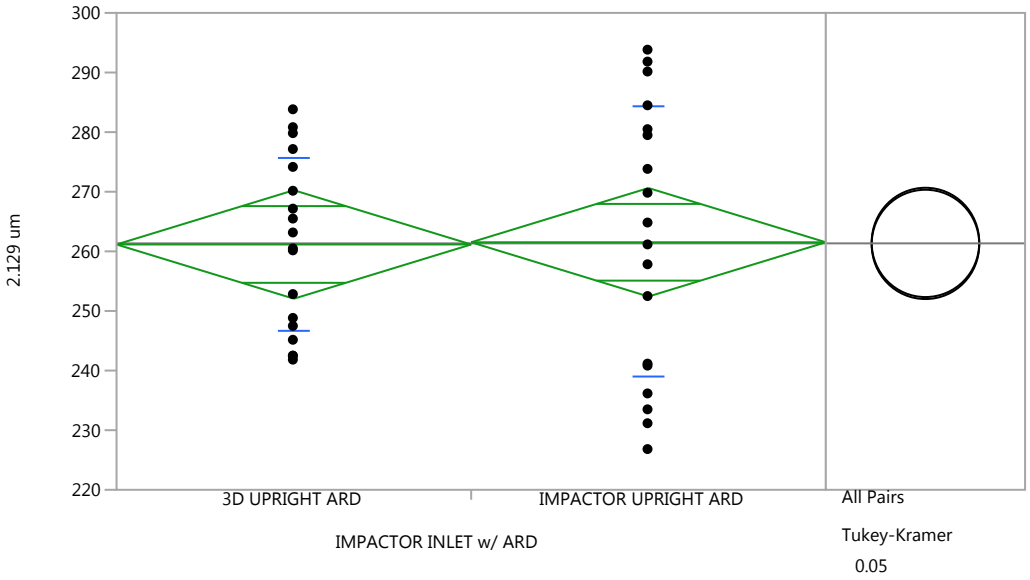


**Figure 54. One-way Analysis of 2.129 µm by 3D Printed Inlet and SKC IMPACT SAMPLER with ARD**

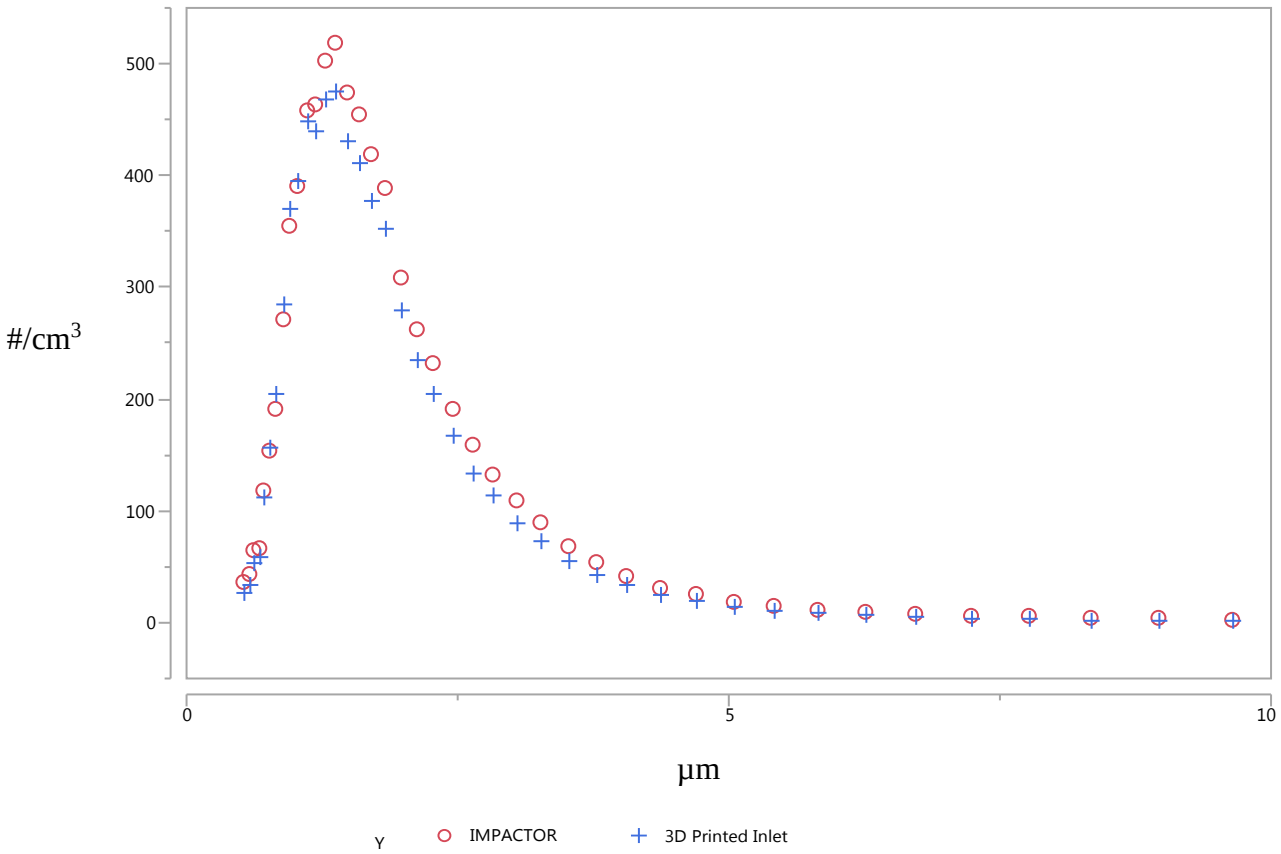


**Figure 55. 3D Printed Inlet and SKC IMPACT SAMPLER Comparison with ARD**

**Summary**

The 3D printed inlet showed a 7.2% negative sampling bias compared to the IMPACT sampler. The design of the inlet utilizing SolidWorks software and ProJet printer was an iterative process. In this study, only one iteration was redesigned and printed. Although, multiple revisions would be necessary to obtain optimal performance. The use of 3D printing allowed for a cost-effective and fast method of inlet design and construction. The electrostatic effects of the plastic material used has yet to be determined, however it was a reasonably robust inlet for aerosol sampling on a UAS.

## VII. Conclusion

The evolving technology of unmanned aerial systems offers a capability for remote sensing and emission monitoring beneficial in the applications of occupational hygiene monitoring. By utilizing a small multi-rotor UAS in aerosol sampling and monitoring, tasks can be accomplished remotely and effectively while limiting hazard exposure. Airflow visualization and velocity measurements aided in the decision of aerosol inlet placement on a UAS platform. The numerical and visual results concluded that directly below the fuselage of the UAS was optimal placement for an air sampling inlet. Varying orientations of the inlets were considered for optimal aerosol sampling when mounted on the UAS. Horizontal orientations of the all three inlets resulted in a negative sampling bias compared to the upright and upside down positions. The results of sampling comparisons while mounted on the UAS suggest that a combination of both the UAS turbulence and wind speed of 0.254 m/s produced a negative sampling bias in all three candidate inlets. To advance the capabilities of aerosol monitoring in occupational hygiene practices, combining the technology of multi-rotor unmanned aerial systems with aerosol sampling devices needs to continue to be explored. Future work includes the determination of sampling efficiencies for each candidate inlet by comparison to an isokinetic reference sampling probe and varying wind speeds to reflect typical workplace conditions and UAS flying weather conditions.

## Bibliography


3D Systems (2015). VisiJet® M3 Black Specifications Sheet. Retrieved November 1, 2016, from https://www.3dsystems.com/materials/visijetr-m3-black

Altstädter B, Platis A, Wehner B et al. (2015). ALADINA–an unmanned research aircraft for observing vertical and horizontal distributions of ultrafine particles within the atmospheric boundary layer. *Atmos Meas Tech*; 8, 1627–39.

Anagnostopoulus, P., Iliadis, G., Richardson., S. (1996). Numerical Study of the Blockage Effects on Viscous Flow Past a Circular Cylinder. *International Journal for Numerical Methods in Fluids*, 22(11), 1061-1074.

Baron, P. A. (2016). Factors Affecting Aerosol Sampling. *NIOSH Manual of Analytical Methods, 5th Edition.*

Bernard PS, Krispin J. (2010). Hazardous particle detection via unmanned air vehicles: optimal placement of sensors in forward flight. *U.S. Army Aviation and Missile Command.* Available at http://www.dtic.mil/dtic/tr/fulltext/u2/a528217.pdf.

Brady, J. (1988). Stokesian Dynamics. *Annual Review of Fluid Mechanics*, 20(1), 111-157. doi:10.1146/annurev.fluid.20.1.111

Brown, J. S., Gordon, T., Price, O., & Asgharian, B. (2013). Thoracic and respirable particle definitions for human health risk assessment. *Particle and Fibre Toxicology*, 10, 12. http://doi.org/10.1186/1743-8977-10-12

Buresti, G. (2000). Bluff-Body Aerodynamics[Lecture Notes]. *International Advanced School on Wind-Excited and Aeroelastic Vibrations of Structures*. Retrieved December 5, 2016, from https://www.mech.kth.se/courses/5C1211/BluffBodies.pdf

Chang, C. C., Wang, J., Chang, C. Y., Liang, M., & Lin, M. (2015). Development of a multi-rotor-carried whole air sampling apparatus and its applications in environmental studies. *Chemosphere*: 144, 484-92.

Chow, J., Watson, J. (1998). Guideline on Speciated Particulate Monitoring. Desert Research Institute. Office of Air Quality Planning and Standards. Retrieved November 1, 2016, from https://www3.epa.gov/ttn/amtic/files/ambient/pm25/spec/drispec.pdf

Corrigan, C. E., Roberts, G. C., Ramana, M. V., Kim, D., & Ramanathan, R. (2008). Capturing vertical profiles of aerosols and black carbon over the Indian Ocean using autonomous unmanned aerial vehicles. *Atmospheric Chemistry and Physics Discussions Atmos. Chem. Phys. Discuss.* 8, 737-747.

Craft, T. L., Cahill, C. F., & Walker, G. W. (2014). Using an unmanned aircraft to observe black carbon aerosols during a prescribed fire at the rxcadre campaign. 2014 International Conference on Unmanned Aircraft Systems (ICUAS), Orlando, 2014. Orlando, FL: Institute of Electrical and Electronics Engineers

Eninger, R. M., & Johnson, R. L. (2015). Unmanned aerial systems in occupational hygiene—learning from allied disciplines. *Annals of Occupational Hygiene*: 59, 949-58.

Görner, P., Wrobel, R., & Simon, X. (2009). High efficiency CIP 10-I personal inhalable aerosol sampler. J. Phys.: Conf. Ser. Journal of Physics: Conference Series, 151, 012061. doi:10.1088/1742-6596/151/1/012061

Harriman, L., & Muhlhausen, J. (2013). A new eye in the sky: Eco-drones. *Environmental Development*: 7, 155-64.

Hermann, M., F. Stratmann, M. W., & Wiedensohler, A. (2001). Sampling characteristics of an aircraft-borne aerosol inlet system. *J. Atmos. Oceanic Technol. Journal of Atmospheric and Oceanic Technology*: 18(1), 7-19.

Hwang, J. Y., Jung, M. K., & Kwon, O. J. (2015). Numerical Study of Aerodynamic Performance of a Multi-rotor Unmanned-Aerial-Vehicle Configuration. *Journal of Aircraft*, 52(3), 839-846. doi:10.2514/1.c032828

John, W., & Kreisberg, N. (1999). Calibration and Testing of Samplers with Dry, Polydisperse Latex. *Aerosol Science and Technology*, 31(2-3), 221-225. doi:10.1080/027868299304264

Jones, A., Aitken, R., Fabriès, J., Kauffer, E., Liden, G., Maynard, A., Riediger, G., & Sahle, W. (2005). Thoracic size-selective sampling of fibres: Performance of four types of thoracic sampler in laboratory tests. *Annals of Occupational Hygiene*, 49(6), 481-492. doi: 10.1093/annhyg/mei004

Kesavan, J., Bottiger, J. (2005). Sampling Efficiency Measurement Methods For Aerosol Samplers. *U.S. Army Research, Development and Engineering Command*. Available at: http://www.dtic.mil/cgi-bin/GetTRDoc?Location=U2&doc=GetTRDoc.pdf&AD=ADA431925

Lee, E., Harper, M., Nelson, J., Hintz, P., Andrew, M. (2008). A Comparison of the CATHIA-T Sampler, the GK2.69 Cyclone and the Standard Cowled Sampler for Thoracic Fiber Concentrations at a Taconite (Iron Ore)-Processing Mill. *Annals of Occupational Hygiene*. 52(1), 55-62. doi: 10.1093/annhyg/mem062

Lee, T., Lee, L., Cauda, E., Hummer, J., Harper, M. (2016). Respirable Size-Selective Sampler for End-of-Shift Quartz Measurement: Development and Performance. *Journal of Occupational and Environmental Hygiene*. doi: 10.1080/15459624.2016.1252845

Lee, T., Kim, S., Chisholm, W., Slaven, J., Harper, M. (2010). Performance of high flow rate samplers for respirable particle collection. *Annals of Occupational Hygiene*. 54 (6), 697-709

Lewis, B. V. (2010). Effects of 0° Cross Draft Velocity and the Presence of a Table and Manikin on Midline Velocities in Front of a Rectangular Capture Hood (Master's thesis). West Virginia University. Publication number:1485740

Maskell, E. C. (1965). A theory of the blockage effects on bluff bodies and stalled wings in a closed wind tunnel. Ministry of Aviation, London, 1965. London, England: Aeronautical Research Council Reports and Memoranda. 3400.

Peck, R., Grinshpun, S., Yermakov, M., Rao, M., Kim, J., Reponen, T. (2016). Efficiency of portable HEPA air purifiers against traffic related combustion particles. *Building and Environment*. 98, 21-29.

Raabe, O. G., & Teague, S. V. (1995). Universal inlet for airborne-particle size-selective sampling. *U.S. Patent No. 5412975*. Washington, DC: U.S. Patent and Trademark Office.

Trakumas, S., Salter, E. (2009). Parallel particle SKC IMPACT sampler – novel size-selective particle sampler for accurate fractioning of inhalable particles. *Journal of Physics: Conference Series.* 151(1), 23-25.

Vincent, J. H. (1995). *Aerosol science for industrial hygienists*. Oxford: Pergamon.

Vincent, J. H. (2007). *Aerosol sampling: science, standards, instrumentation and applications.* Chichester, England: John Wiley & Sons.

Volkwein J., Maynard A., Harper M. (2011) In Kulkami P, Baron PA, Willeke K (Editors) A*erosol measurement: principles, techniques, and applications*. 3rd Edition. Hoboken, New Jersey: John Wiley & Sons.

Watts, A. C., Ambrosia, V. G., & Hinkley, E. A. (2012). Unmanned aircraft systems in remote sensing and scientific research: classification and considerations of use. *Remote Sensing*: 4(4), 1671-692.

# REPORT DOCUMENTATION PAGE

*Form Approved*
*OMB No. 0704-0188*

Public reporting burden for this collection of information is estimated to average 1 hour per response, including the time for reviewing instructions, searching existing data sources, gathering and maintaining the data needed, and completing and reviewing this collection of information. Send comments regarding this burden estimate or any other aspect of this collection of information, including suggestions for reducing this burden to Department of Defense, Washington Headquarters Services, Directorate for Information Operations and Reports (0704-0188), 1215 Jefferson Davis Highway, Suite 1204, Arlington, VA 22202-4302. Respondents should be aware that notwithstanding any other provision of law, no person shall be subject to any penalty for failing to comply with a collection of information if it does not display a currently valid OMB control number.
**PLEASE DO NOT RETURN YOUR FORM TO THE ABOVE ADDRESS.**

| | | |
|---|---|---|
| **1. REPORT DATE** *(DD-MM-YYYY)*<br>23-03-2017 | **2. REPORT TYPE**<br>Master's Thesis | **3. DATES COVERED** *(From - To)*<br>August 2015 – March 2017 |
| **4. TITLE AND SUBTITLE**<br>Optimal Configurations For Aerosol Monitoring With Multi-Rotor Small Unmanned Aerial Systems | | **5a. CONTRACT NUMBER**<br>**5b. GRANT NUMBER**<br>**5c. PROGRAM ELEMENT NUMBER** |
| **6. AUTHOR(S)**<br>Chavez, Inna D., Captain, USAF | | **5d. PROJECT NUMBER**<br>**5e. TASK NUMBER**<br>**5f. WORK UNIT NUMBER** |
| **7. PERFORMING ORGANIZATION NAME(S) AND ADDRESS(ES)**<br>Air Force Institute of Technology<br>Graduate School of Engineering and Management (AFIT/EN)<br>2950 Hobson Way<br>Wright-Patterson AFB OH 45433-7765 | | **8. PERFORMING ORGANIZATION REPORT NUMBER**<br>AFIT-ENV-MS-17-M-179 |
| **9. SPONSORING / MONITORING AGENCY NAME(S) AND ADDRESS(ES)**<br>AFIT Faculty Research Council<br>AFIT/ENRS, 2950 Hobson Way<br>Wright-Patterson AFB, OH 45433-7765<br>(937) 255-3633, (937) 656-7139 fax | | **10. SPONSOR/MONITOR'S ACRONYM(S)**<br>**11. SPONSOR/MONITOR'S REPORT NUMBER(S)** |

**12. DISTRIBUTION / AVAILABILITY STATEMENT**
DISTRIBUTION STATEMENT A. APPROVED FOR PUBLIC RELEASE; DISTRIBUTION UNLIMITED.

**13. SUPPLEMENTARY NOTES**
This material is declared a work of the U.S. Government and is not subject to copyright protection in the United States.

**14. ABSTRACT**
Applicability of aerosol sampling on multi-rotor unmanned aerial systems (UAS) platform was investigated. Multi-rotor UAS have impacts of wind speed, turbulence, and orientation possibly contributing to sampling bias. The SKC IMPACT sampler, Tecora C.A.Th.I.A., and modified three-dimensionally printed Universal Inlet for Airborne-Particle Size-Selective Sampling were selected based on particle size-selectivity and operational independence to wind. Airflow visualizations concluded that below UAS fuselage was optimal sampler placement. Tests were conducted with Arizona Road Dust in a still-air chamber, and aerosolized sugar in a wind tunnel. Inlet mounting was evaluated in, upright, upside-down, and horizontal orientations. Horizontal orientations of all inlets resulted in negative sampling bias compared to upright/upside-down positions. Sampling bias of inlets mounted on the UAS were compared with and without motor employment. In wind tunnel tests, the IMPACT sampler averaged lowest count concentration bias while the 3D printed inlet resulted in the largest percent difference. Results suggests, UAS turbulence and low wind speed produced negative sampling bias. The 3D printed inlet was designed with Stokes' scaling factor, and compared with the well-characterized IMPACT sampler. Three-dimensional printing bolstered a cost-effective and fast method of inlet design and construction. Iterative designs can optimize aerosol inlets suitable for mounting on multi-rotor UAS.

**15. SUBJECT TERMS**
Unmanned aerial systems, aerosols, aerosol sampling, sampling efficiency, particle size-selective inlets

| **16. SECURITY CLASSIFICATION OF:** | | | **17. LIMITATION OF ABSTRACT** | **18. NUMBER OF PAGES** | **19a. NAME OF RESPONSIBLE PERSON** |
|---|---|---|---|---|---|
| | | | | | Lt Col Robert Eninger, AFIT/ENV |
| **a. REPORT** | **b. ABSTRACT** | **c. THIS PAGE** | UU | 87 | **19b. TELEPHONE NUMBER** |
| U | U | U | | | (937)-255-3636 ext. 4511 robert.eninger@afit.edu |

**Standard Form 298 (Rev. 8-98)**
**Prescribed by ANSI Std. Z39.18**